Climate Dynamics (2019) 53:3985–4004
https://doi.org/10.1007/s00382-019-04766-5

Factors affecting interdecadal variability of air–sea CO_2 fluxes in the tropical Pacific, revealed by an ocean physical–biogeochemical model

Feng Tian[1,2] · **Rong-Hua Zhang**[1,2,3,4] · **Xiujun Wang**[5]

Received: 27 July 2018 / Accepted: 8 April 2019 / Published online: 16 April 2019

Abstract

The tropical Pacific is the largest source region of CO_2 release to the atmosphere through the sea surface, with air–sea CO_2 fluxes varying on seasonal to interdecadal timescales, which is attributed to several factors. At present, there is no consensus on the relative contributions of wind speed and ΔpCO_2 (the partial pressure of CO_2 [pCO_2] difference between sea surface and the atmosphere) to the interdecadal variability of CO_2 fluxes, especially concerning their linkage with the Interdecadal Pacific Oscillation (IPO). By using a coupled ocean physical–biogeochemical model forced by the NCEP/NCAR winds during 1958–2016, we show that the CO_2 fluxes exhibit interdecadal regime shifts in 1975–1976 and 1997–1998, which is coincident with the regime transitions of the IPO. Furthermore, the interdecadal variability of wind speed is demonstrated to play a significant role in determining the magnitude and location of interdecadal variability of CO_2 fluxes, while the contribution of ΔpCO_2 is relatively small. Additionally, the location of maximum variability of CO_2 fluxes gradually migrates westward during 1958–2016, which is related to the interdecadal change in the relationship between wind speed and CO_2 fluxes. Modelling results suggest that the regime shifts of CO_2 fluxes in the future decades may significantly influence the projection of long-term trend in CO_2 fluxes in the tropical Pacific Ocean.

Keywords Tropical Pacific · Interdecadal variability of air–sea CO_2 fluxes · Regime shift · Wind speed · Ocean physical–biogeochemical model

1 Introduction

The equatorial Pacific is the major source region for outgassing CO_2 to the atmosphere, annually amounting to 0.44 ± 0.14 PgC (Feely et al. 1999; Ishii et al. 2014). In this region, CO_2 exhibits multiple variability from interannual to interdecadal timescales. On interannual timescale, El Niño-Southern Oscillation (ENSO) influences strengths of trade winds and upwelling in the central and eastern equatorial Pacific, and further affects marine primary production and carbon cycle (Landschützer et al. 2014; Zhang and Gao 2016; Kang et al. 2017). Previous studies (e.g. Feely et al. 1999, 2006; Rayner et al. 1999; Le Quéré et al. 2000; Wanninkhof et al. 2013) have demonstrated that interannual variability of CO_2 fluxes in this region accounts for 70% of that in the global ocean. On decadal timescales, major physical and biological changes are evident over the Pacific basin. An example for this fluctuation is commonly called as the interdecadal Pacific Oscillation (IPO) in the climate community (Power et al. 1999; Newman et al. 2003; Liu 2012; Meehl et al. 2016). The IPO experienced two pronounced regime shifts in 1975–1977 and 1997–1998, which is clearly represented in anomalies of sea surface temperature, wind stress and even fish production (e.g. Mantua et al. 1997). For instance, the negative (cooling) phase of the IPO after

✉ Rong-Hua Zhang
rzhang@qdio.ac.cn

1 CAS Key Laboratory of Ocean Circulation and Waves, Institute of Oceanology, Chinese Academy of Sciences, Qingdao 266071, China

2 University of Chinese Academy of Sciences, Beijing 10029, China

3 Pilot National Laboratory for Marine Science and Technology, Qingdao, China

4 Center for Ocean Mega-Science, Chinese Academy of Sciences, 7 Nanhai Road, Qingdao 266071, China

5 College of Global Change and Earth System Science, Beijing Normal University, Beijing 100875, China

1999 is associated with a cooling trend in the eastern tropical Pacific that has contributed to recent global warming hiatus (Kosaka and Xie 2013; England et al. 2014). Although the cause and influence of the IPO have been widely investigated and understood qualitatively (e.g. Trenberth and Hurrell 1994; Power et al. 1999; Zhang et al. 1999; Choi et al. 2012; Han et al. 2014; Chen and Tung 2018; Tung et al. 2019), large uncertainties exist in the magnitudes of interdecadal variations in CO_2 fluxes owing to the limitation of observed data and model developments (e.g. Patra et al. 2005; Wetzel et al. 2005; Feely et al. 2006; Doney et al. 2009; Ishii et al. 2009, 2014; Wanninkhof et al. 2013; Fay and McKinley 2013; Valsala et al. 2014; Xiu and Chai 2014; Dunne et al. 2015; McKinley et al. 2017).

In addition to the uncertainty in the variability of CO_2 fluxes, the mechanisms affecting interdecadal variability of CO_2 fluxes are still not understood well. The CO_2 fluxes at the air–sea interface are determined by several factors, including the pCO_2 difference (ΔpCO_2, pCO_2 at the sea surface minus pCO_2 in the atmosphere), wind speed, temperature and salinity (Wanninkhof et al. 2009). In addition, the sign of CO_2 fluxes between ocean and atmosphere is determined by ΔpCO_2. Because the spatio-temporal variability of atmospheric CO_2 is relatively small, the variability of ΔpCO_2 reflects mainly in the sea surface pCO_2. In quantifying oceanic role, the decadal variability of sea surface pCO_2 was also investigated by several modelling studies (Valsala et al. 2014; Wang et al. 2015). Model results demonstrated that ocean dynamics induced change in dissolved inorganic carbon (DIC) plays a key role in determining the decadal variability of pCO_2. For instance, Valsala et al. (2014) found that decadal change in DIC can be traced to the North Pacific through thermocline pathway. By using a biogeochemical model, Wang et al. (2015) demonstrated that the equatorial Pacific is a DIC-driven system of carbon cycle on decadal timescale, but the mechanism for controlling carbon system variability on interdecadal timescale has not been investigated adequately.

The CO_2 fluxes are also strongly influenced by wind speed in addition to ΔpCO_2, and the contributions from temperature and salinity to CO_2 fluxes are relatively small. This is because the products of gas transfer velocity and solubility, the factors affecting CO_2 fluxes, have weak dependence on temperature (Wanninkhof and Triñanes 2017). On interdecadal timescale, the IPO plays a significant role in affecting the Walker Circulation in the Pacific. For example, during the recent decade of this century, the unprecedented intensification of trade winds associated with the cooling phase of the IPO is anticipated to affect the CO_2 fluxes in the Pacific through the variability of wind speed (England et al. 2014; Bordbar et al. 2017). Wanninkhof and Triñanes (2017) found that the increasing of wind speed led to an increase in efflux of CO_2 in the equatorial Pacific by 0.03–0.04 PgC decade^{-1} during 1988–2014. Subsequently, the net CO_2 uptake of global ocean slightly decreases by 0.00–0.02 PgC decade^{-1}. Feely et al. (2006) suggested that the increased CO_2 fluxes were due to the increase in wind speeds after the spring of 1998 when regime of the IPO shifted from positive (warm) phase to negative (cold) phase. However, the relative contributions of wind speed and ΔpCO_2 to the interdecadal variability of CO_2 fluxes have not been quantified. Moreover, due to quadratic dependence of CO_2 fluxes (FCO_2) on wind speed (u) ($FCO_2 \propto u^2$), the increased frequency of La Niña events during the IPO cold phase may lead to an increase in wind speed and further an increase in CO_2 fluxes on interdecadal timescale. This study will mainly focus on these issues.

Previous studies have focused more on the recent regime shift during 1997–1998, but less on the earlier regime shift during 1975–1977. In addition, the magnitude of the interdecadal variability of CO_2 fluxes and the underlying mechanism are not clear. The observational data of CO_2 fluxes are only available from 1970s; relatively short time series may not be sufficient to depict the regime shift of CO_2 fluxes on decadal timescale. The biogeochemical modeling is an alternative way to study interdecadal variability of air–sea CO_2 fluxes and its relationships with climatic variability like the IPO. In this study, we investigate the interdecadal variability of CO_2 fluxes and possible mechanisms responsible for it, using a fully coupled ocean physics–biogeochemical model forced by NCEP/NCAR winds during 1948–2016.

The paper is organized as follows. Section 2 describes the model setup and dataset used for validation. Section 3 examines the interdecadal variability of CO_2 fluxes and the roles played by wind and ΔpCO_2 in the variability. A discussion is given in Sect. 4, and a summary is presented in Sect. 5.

2 Model description and data used

2.1 Ocean general circulation model

The ocean general circulation model (OGCM) used in this study is a primitive equation model (sigma-coordinate, reduced-gravity), specificially developed for the upper equatorial ocean (Gent and Cane 1989). An advective atmosphere mixed layer model for calculating sea surface heat fluxes (Seager et al. 1995; Murtugudde et al. 1996) is coupled with the OGCM. The model domain covers the entire tropical Pacific basin (120°E–76°W, 30°S–30°N). The model has 20 vertical layers with variable thicknesses; a mixed layer at the top is determined by a mixed layer model (Chen et al. 1994). The zonal resolution of this model is 1° in the central basin and gradually increases to 0.4° in the western and eastern boundaries. The meridional resolution is from 0.3° to 0.6° between 15°S and 15°N and gradually decreases to 2° at the northern and southern boundaries. Sponge layers are set within the 10° domain near the northern and southern boundaries. Some physical and biological variables (e.g. temperature, salinity, and nitrate) are gradually relaxed back to their corresponding climatological fields from WOA98 atlas (http://www.nodc.noaa.gov/OC5/indprod.html).

The model is initialized by temperature and salinity from the World Ocean Atlas data (WOA01) and spun up for 30 years under atmospheric climatological forcing. Subsequently, the model is integrated from 1948 to 2016, forced by daily wind fields from the National Centers for Environmental Prediction/National Center for Atmospheric Research (NCEP/NCAR) reanalysis (Kalnay et al. 1996), and the climatological fields of solar radiation, clouds and precipitation. The monthly output during the period of 1958–2016 is used for our analyses.

2.2 A carbon chemistry model

The biogeochemical model consists of 12 components, including six biological components [large (L) and small (S) size classes of phytoplankton (P), zooplankton (z) and detritus (D)] and six kinds of nutrients (nitrate, ammonium, dissolved oxygen, silicon, dissolved inorganic carbon (DIC), and dissolved iron). The model equations and structure were detailed by Wang et al. (2008). The vertical mixing parametrization schemes for all biological components are similar to those for temperature and salinity at each layers (Chen et al. 1994), with unified units being used by mol N m^{-3}.

The carbon chemistry model embedded in the ocean physical model had been described in Wang et al. (2006, 2015). Briefly, CO_2 fluxes (FCO_2) from sea surface into the atmosphere are calculated as follows;

$$FCO_2 = SK_0 \Delta pCO_2 \tag{1}$$

where S is the solubility of CO_2 calculated from temperature and salinity; K_0 is the gas transfer velocity (Wanninkhof 1992)

$$K_0 = 0.31u^2 \left(\frac{Sc}{Sc_{20}} \right)^{-\frac{1}{2}} \tag{2}$$

where u is wind speed from the NCEP/NCAR reanalysis and Sc is the Schmidt number; ΔpCO_2 represents the difference in pCO_2 between sea surface and the atmosphere. The atmospheric pCO_2 data are taken from http://aftp.cmdl.noaa.gov/products/trends/CO2/CO2_annmean_mlo.txt during 1948–2016. The alkalinity is calculated based on the salinity–alkalinity relationship derived from the Pacific GLODAP bottle data (http://cdiac.ornl.gov/oceans/glodap/).

2.3 Coupling between physics and biogeochemistry in the model

Recently, we updated the model to investigate the interaction between ocean physics and biogeochemistry in the tropical Pacific (Zhang et al. 2018a, b). A parameterization scheme is introduced to represent chlorophyll induced heating effect on the upper ocean (Wang et al. 2008; Zhang 2015), which is allowed to affect ocean thermodynamics and further change in the biogeochemical condition. Therefore, this new model adopts a two-way coupling strategy between physical and biogeochemical processes. As a result, this coupling allows for bio-feedback onto temperature, stratification, and mixing (Zhang et al. 2018a), which can further affect the solubility of pCO_2 in the seawater (solubility pump) and ocean stratification.

2.4 Data

Monthly sea surface temperature data are taken from Extended Reconstructed Sea Surface Temperature, Version 5 (ERSSTv5) over the period of 1958–2016 (Huang et al. 2017). Annual mean CO_2 fluxes data is from Global Surface pCO_2 Database V2016 at Lamont–Doherty Earth Observatory (LDEO), Columbia University (Takahashi et al. 2009). Besides, an updated observation-based global monthly gridded air–sea CO_2 fluxes product (Landschützer et al. 2016) is used to validate the model simulations. This pCO_2 product is based on a two-step neural network approach to extrapolate the monthly gridded SOCAT v4 product (Bakker et al. 2016). Next, sea–air CO_2 flux maps are computed using a standard bulk formulation and high-resolution wind speeds, with the spatial resolution of $1° \times 1°$ and time range being from 1982 to 2015.

3 Results

3.1 Model validation

We first use the Annual Flux Gridded Database (Takahashi et al. 2009) to validate annual mean CO_2 fluxes in the model simulation. As displayed in Fig. 1a, b, the model captures the spatial pattern of annual mean CO_2 fluxes quite well in the equatorial Pacific. Positive values indicate that ocean release CO_2 to the atmosphere. For the observation, regions with large CO_2 fluxes are seen in the southeastern tropical Pacific and those with low values are seen in the western equatorial and subtropical Pacific. These observed features are faithfully captured by the model, although the simulated annual mean CO_2 fluxes are slightly higher than observation

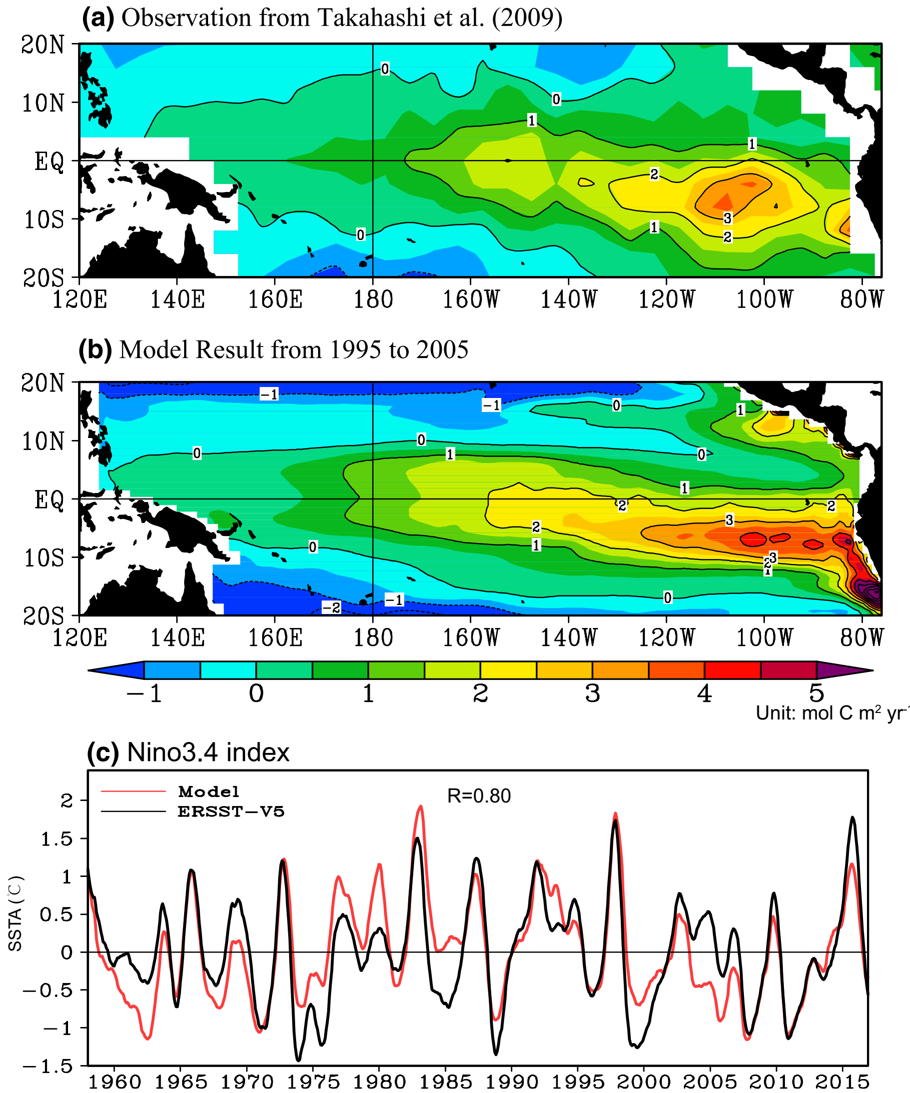

Fig. 1 Annual mean of sea-air CO_2 fluxes during 1995–2005 from Takahashi et al. (2009) database (**a**), and from model results (**b**). **c** Niño3.4 SST anomalies from ERSST-V5 (black line) and model results (red line) during the period of 1958-2016. The positive value denotes the oceanic releases of CO_2 to the atmosphere and negative value denotes the oceanic absorption of CO_2. The contour interval is 1 mol C m^{-2} $year^{-1}$ in **a** and **b**

in the southeastern tropical Pacific (Fig. 1b). This model bias may be related to strong upwelling represented in the ocean model simulation.

To evaluate the model performance in simulating interannual to interdecadal variability of SST in the tropical Pacific, we compared the simulated SST with that in ERSST-v5 through calculating detrended Niño3.4 index from 1958 to 2016 (Fig. 1c). The model can well reproduce the main ENSO events (e.g. 1997–1998 El Niño event). The correlation coefficient reaches 0.80 between modeled and observed Niño3.4 index, indicating that model outputs can be used to investigate interannual to interdecadal variability in the tropical Pacific.

Furthermore, we examined the decadal variability of CO_2 fluxes by comparing the simulated decadal mean CO_2 fluxes to observation from Ishii et al. (2014) during the periods of 1990–1999 and 2000–2009. The data in Ishii et al. (2014) are obtained from various approaches (observation-based and biogeochemical model products) (Table 1). The decadal mean values of air–sea CO_2 fluxes simulated by the model are 0.41 ± 0.14 PgC $year^{-1}$ during 1990–1999 and

Table 1 Decadal mean values of air–sea CO_2 fluxes in the equatorial Pacific (18°S–18°N) from various studies calculated during two periods (1990–1999, 2000–2009). (Units: PgC $year^{-1}$)

Periods	Ishii et al. (2014)		This study
	pCO_2sw Diag. Models[a]	OBGC Models[b]	NCEP-forcing
1990–1999	$+0.49 \pm 0.07$	$+0.36 \pm 0.06$	0.41 ± 0.14
2000–2009	$+0.56 \pm 0.11$	$+0.41 \pm 0.04$	0.53 ± 0.16

[a] The analysis here draws upon the datasets of gridded monthly climatological pCO_2sw in the reference year 2000 (Takahashi et al. 2009)

[b] The data are from several prognostic ocean biogeochemistry/general circulation model simulations over the period of interest (see details in Ishii et al. 2014)

0.53 ± 0.16 PgC year^{-1} during 2000–2009, respectively. This decadal change in CO_2 fluxes is associated with the phase change in the IPO, and is in good agreement with the observation-based estimate ($+0.49 \pm 0.07$ PgC year^{-1} and $+0.56 \pm 0.11$ PgC year^{-1}, respectively). In addition, as shown in Fig. 2, we compared the tropical Pacific CO_2 fluxes from model output with an observation-based global monthly gridded product for air–sea CO_2 fluxes (Landschützer et al. 2016) during 1982–2015. Figure 2 shows that seasonal to decadal variabilities of CO_2 fluxes are well-correlated (correlation coefficient of 0.57) between observation-based product and model output in the entire tropical Pacific (120°E–80°W, 18°S–18°N) (Fig. 2a). Meanwhile, the correlation coefficients are 0.46 and 0.91 in the Niño3 region (150°W–90°W, 5°S–5°N) and Niño4 region (160°E–150°W, 5°S–5°N), indicating that model can well capture the variability of CO_2 fluxes in the tropical Pacific, especially in the western-central equatorial Pacific (Fig. 2b, c).

3.2 Interdecadal variability of CO_2 fluxes: two regime shifts

Figure 3a shows that CO_2 fluxes in the equatorial Pacific experienced two pronounced decadal shifts during the period

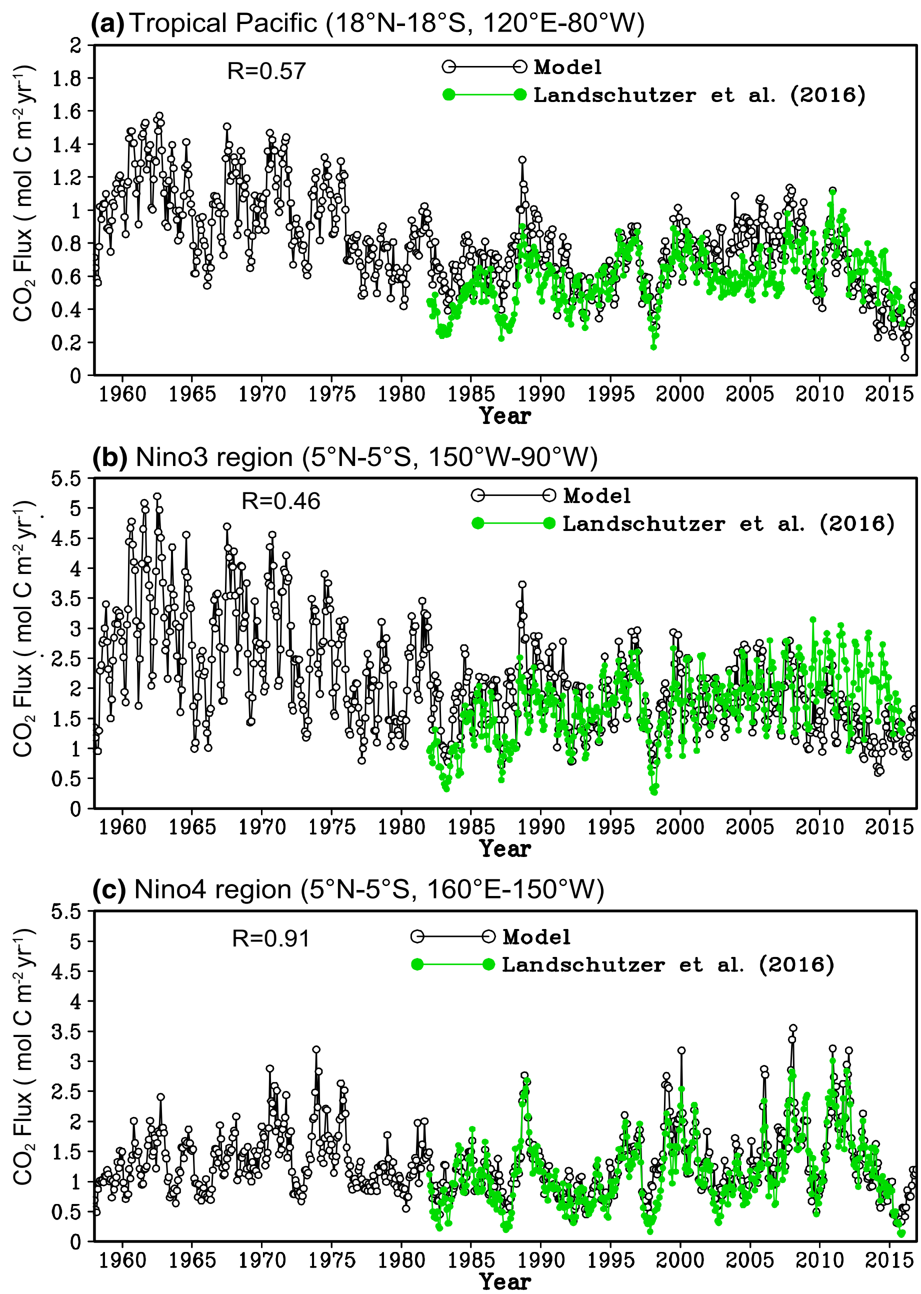

Fig. 2 Comparisons of integrated CO_2 fluxes between model and observation-based air–sea CO_2 flux product (Landschützer et al. 2016) for **a** in the entire tropical Pacific (120°E–80°W, 18°S–18°N), (b) the Niño3 region (150°W–90°W, 5°S–5°N), and **c** the Niño4 region (160°E–150°W, 5°S–5°N). The corresponding correlation coefficients are given

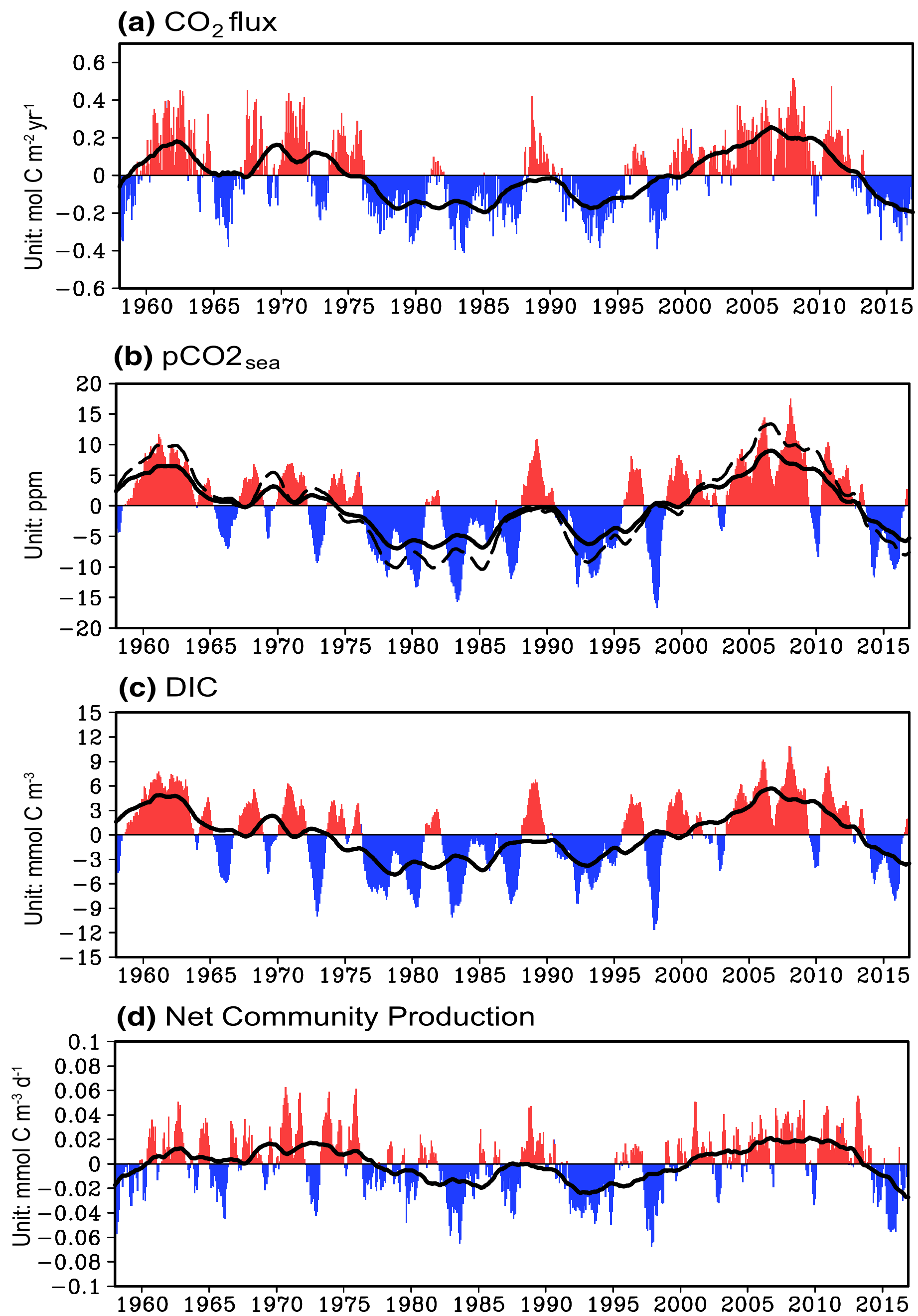

Fig. 3 The modeled detrended interannual anomalies of sea-to-air CO_2 fluxes (**a**), sea surface pCO_2 (**b**), DIC (**c**) and NCP (**d**) during the period of 1958–2016 in the tropical Pacific (120°E–80°W, 18°S–18°N). The black line denotes the 5-year running mean for interannual anomalies. Note the black dashed line in **b** is sea surface pCO_2 at 25 °C. The units are mol C m^{-2} $year^{-1}$ in **a**, ppm in **b**, mmol C m^{-3} in **c** and mmol C m^{-3} $days^{-1}$ in **d**

1958–2016. The first one occurred in 1975–1976 when the IPO shifted from cold phase (1958–1975) to warm phase (1976–1997). This period was characterized by a decrease in CO_2 fluxes nearly by 0.4 mol C m^{-2} $year^{-1}$ during the period of 1976–1997. During this period, the slowdown of shallow meridional overturning circulation lead to surface warming by 1 °C (Zhang and Levitus 1997; McPhaden and Zhang 2002) and a decrease in DIC by 5–10 mmol m^{-3} (Fig. 3c). In addition, El Niño events occur frequently during this positive IPO phase, and lead to a decrease in wind speed by 1–2 m s^{-1} (Fig. 4). As shown in Fig. 4a, central Pacific (CP) El Niño type occurred frequently during recent decades, which is characterized by positive SST anomaly being concerntrated in the central equatorial Pacific (e.g. Ashok and Yamagata 2009; Kug et al. 2009; Yu and Kim 2010). Consequently, large interannual anomaly center of wind speed tends to be located near the dateline (Fig. 4b). The decrease in wind speed can reduce the outgassing of CO_2 from sea surface during El Niño events (Figs. 4b, 5b). Subsequently, the maximum variability region of CO_2 flux migrates westward gradually during this period (Fig. 5b). Meanwhile, the regime shift of ΔpCO_2 is similar to that of DIC, suggesting that interdecadal phase change of DIC has an important influence on that of ΔpCO_2 (Figs. 3b, c, 5a).

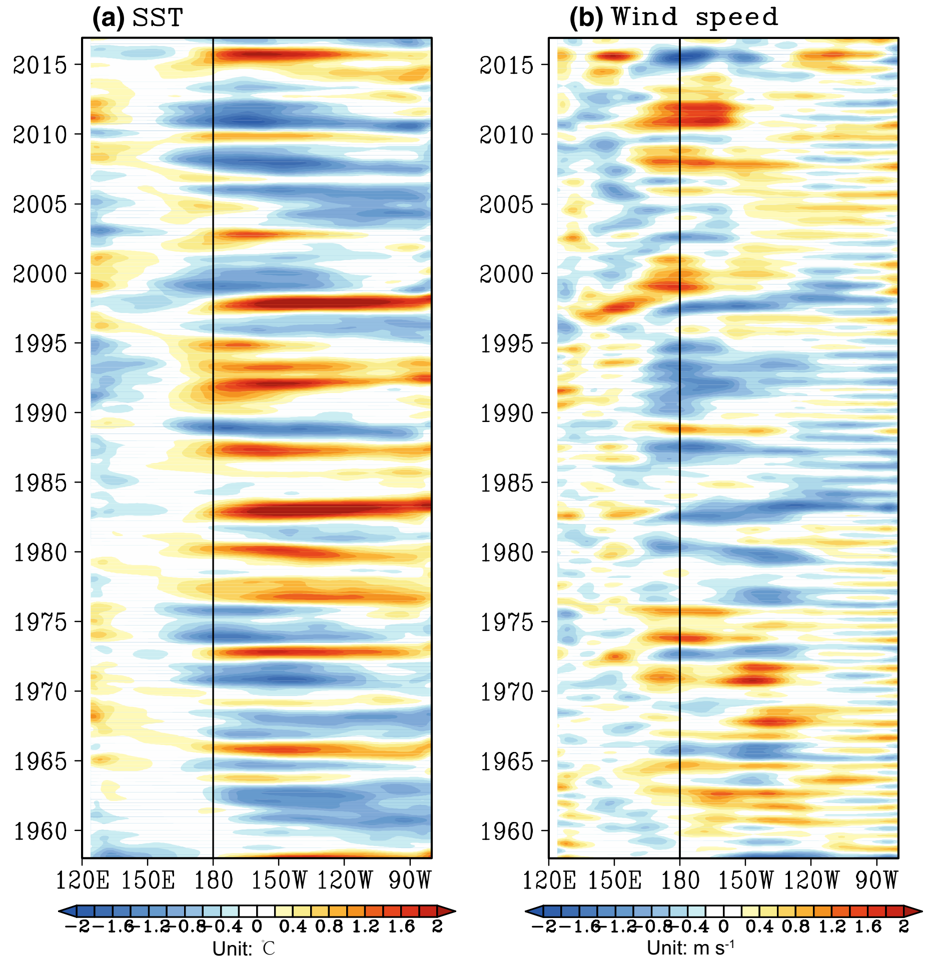

Fig. 4 The interannual anomalies along the equator for SST (**a**) and wind speed from NCEP/NCAR reanalysis (**b**) during the period 1958–2016. The long-term trends are removed. The units are °C in **a** and m s^{-1} in **b**

The second regime shift took place around 1997–1998. Recent similar studies showed that the outgassing fluxes of CO_2 appeared to have a slight increase in the equatorial Pacific when the IPO regime shifted from warm phase (1976–1997) to cold phase (1998–2012) during 1997–1998 (Feely et al. 2006). Since 1998, the tropical Pacific trade winds strengthened again and wind-driven circulation spun up, with the surface cooling emerged in the central and eastern equatorial Pacific (Fig. 4a) (Kosaka and Xie 2013; England et al. 2014). The increase in trade winds led to an increase in CO_2 fluxes during this IPO phase (Figs. 3a, 5b). Contrasts to the former cold phase of the IPO (1958–1975), large SST anomaly regions are confined more to the central Pacific during this IPO cold phase. This is because the frequencies of La Niña increase during the IPO cold phase, with the cold SST anomalies during La Niña tending to be more westward than positive SST anomalies during El Niño. Figures 4b and 5b show that positive anomalies of CO_2 fluxes are associated with an increase in wind speed in the central Pacific during La Niña events (Fig. 4b). The increased frequency of La Niña further leads to an increase in CO_2 fluxes through the amplifying effect of wind speed during this IPO cold phase. Because the frequencies of El Niño (La Niña) occurring can be modulated by background state (warming or cooling trend) of the tropical Pacific on interdecadal timescale (Lin et al. 2018; An 2018), the interdecadal variability of CO_2 fluxes is tightly associated with ENSO frequency and asymmetry on interdecadal timescale. In addition, the increased La Niña events during the IPO cold phase further result in westward migration of maximum anomalies for CO_2 fluxes. However, the interannual anomalies of ΔpCO_2 are mainly located in the eastern Pacific (Fig. 5a), indicating that ΔpCO_2 may have little influence on interannual variability of CO_2 fluxes during this IPO phase.

Besides the physical factors, the biological activity also exhibits distinguished interdecadal fluctuations. Figure 3d shows that net community production (NCP) decreases in the warm phase but increases in the cold phase of the IPO, although the timing of regime shift slightly lags behind the other process like DIC by 1–2 years (e.g. the regime shift of NCP occurred in 2000–2001). The NCP represents the net change of DIC at the sea surface due to the biological uptake and regeneration (Wang et al. 2006). Therefore, the interdecadal variability of NCP can exert influence on seawater

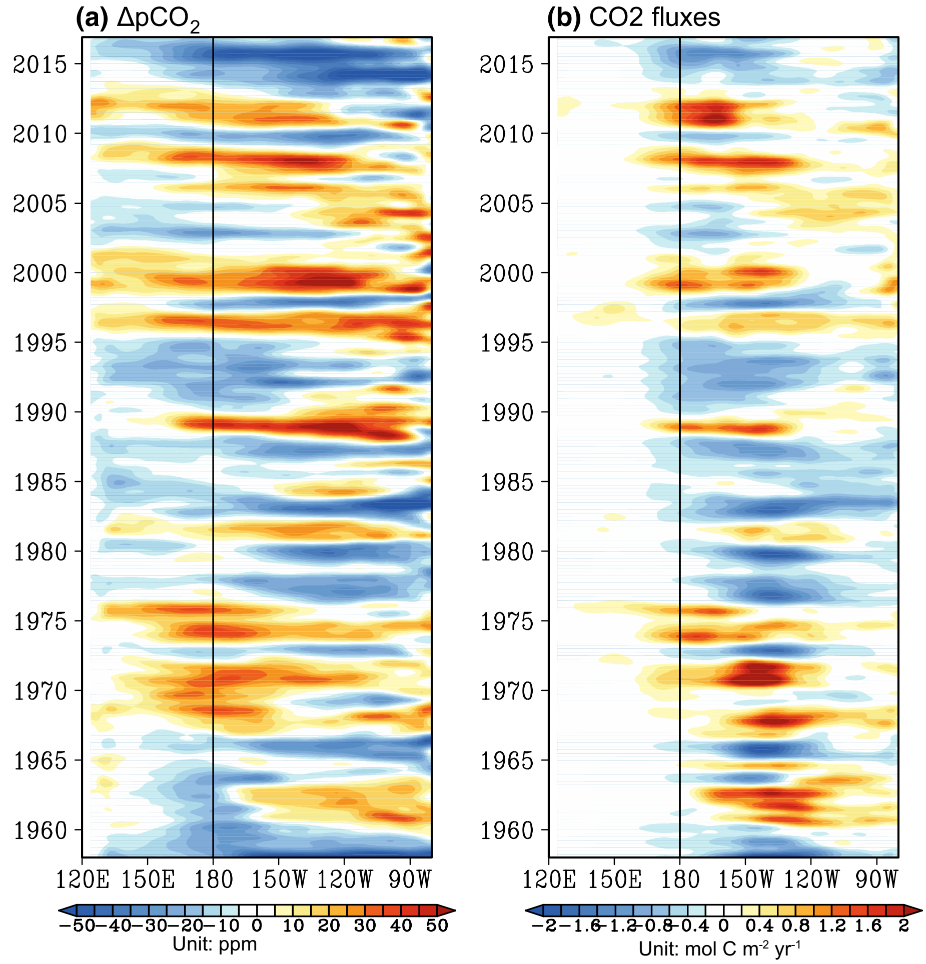

Fig. 5 The interannual anomalies along the equator for ΔpCO_2 (**a**) and CO_2 fluxes (**b**) during the period 1958-2016. The long-term trends are removed. The units are ppm in **a** and mol C m^{-2} $year^{-1}$ in **b**

pCO_2 by removing DIC in the mixed layer. The details of how NCP affects pCO_2 will be explored further below.

3.3 Interdecadal changes in the relationships of CO_2 fluxes with wind speed and ΔpCO_2 anomalies

Because CO_2 fluxes are mainly determined by wind speed and ΔpCO_2, the interdecadal changes in the relationships between the CO_2 fluxes and wind speed or ΔpCO_2 can be further estimated by a regression analysis. According to the timing of regime shifts for CO_2 fluxes (Fig. 3a), we divided the entire period (1958–2016) into three sub-periods, i.e. 1958–1975, 1976–1997, and 1998–2012. The recent period of 2013–2016 was not taken into account so that the influence of the extreme El Niño in 2015–2016 on the analysis results is excluded (Zhang and Gao 2016; Hu and Fedorov 2017). In addition, regression analysis is conducted in the Niño4 region (160°E–150°W, 5°S–5°N) and the Niño3 region (170°W–120°W, 5°S–5°N), respectively. As indicated in Fig. 6a, the regression coefficients between CO_2 fluxes and wind speed are 0.57, 0.41, and 0.65 mol C m^{-2} $year^{-1}$ per 1 m s^{-1} in the Niño4 region during the period of 1958–1975, 1976–1997, and 1998–2012, respectively. Thus, the regression coefficients exhibit clearly interdecadal fluctuations associated with the IPO phases. Given the same wind speed anomaly, the amplitude of variability in CO_2 fluxes due to the wind speed anomalies can be increased during the IPO cold phase in the western-central equatorial Pacific, but decreased during the IPO warm phase.

In the eastern equatorial Pacific (Fig. 6b), the regression coefficients between CO_2 fluxes and wind speed decrease unanimously during these periods and exhibit no interdecadal phase change (i.e. the regression coefficients are 1.4, 1.3 and 0.9 mol C m^{-2} $year^{-1}$ per 1 m s^{-1} in the Niño3 region during the period 1958–1975, 1976–1997 and 1998–2012, respectively). Thus, the regression coefficients increase in the western-central Pacific, but decrease in the eastern Pacific during these three sub-periods. It is suggested that the possible influence of global warming tends to enhance (weaken) the relationship between CO_2 fluxes and wind speed in the western-central (eastern) Pacific. Meanwhile, the annual mean values of CO_2 fluxes during these three periods exhibit clear interdecadal shifts in the Niño4 region (1.40, 1.10, 1.56 mol C m^2 $year^{-1}$ during 1958–1975,

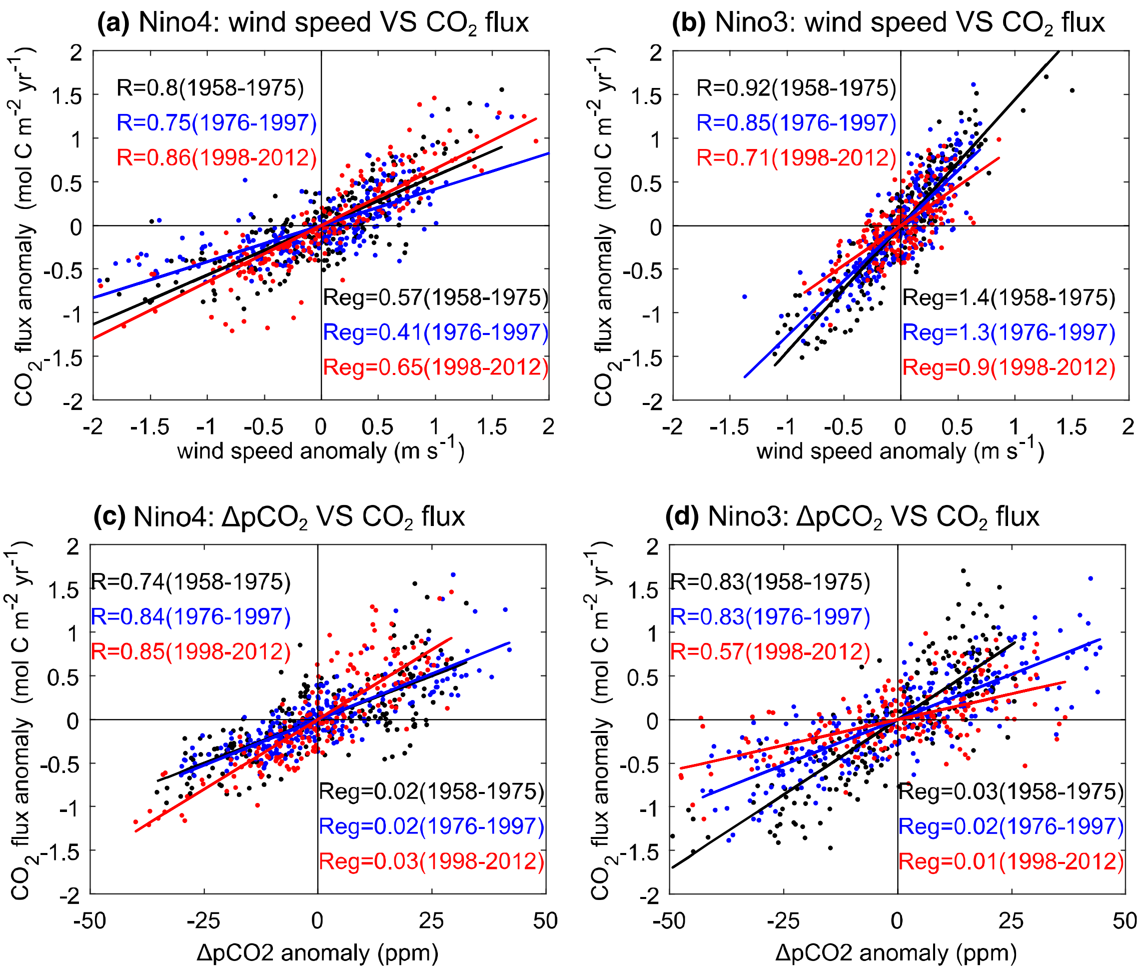

Fig. 6 Scatterplots for anomalies of the wind speed and of CO_2 fluxes in the Niño4 (**a**) and Niño3 region (**b**), which are separately illustrated during the three periods (1958–1975, 1976–1997 and 1998–2012). **c**, **d** are similar to **a**, **b** but for those of the ΔpCO_2 and CO_2 fluxes

1976–1997 and 1998–2012). However, as indicated in the Niño3 region, the interdecadal shifts of CO_2 fluxes are not clearly represented (2.89, 1.87, 1.76 mol C m^2 $year^{-1}$ during 1958–1975, 1976–1997 and 1998–2012) (Table 2).

The similar regression analyses are conducted between ΔpCO_2 and CO_2 fluxes (Fig. 6c, d). Figure 6c shows that regression coefficients are 0.02, 0.02, and 0.03 mol C m^{-2} $year^{-1}$ per ppm in the Niño4 region during the period 1958–1975, 1976–1997 and 1998–2012, respectively. This indicates the relatively weak influence of ΔpCO_2 on the interdecadal shift of CO_2 fluxes variability in the western-central Pacific. In the eastern equatorial Pacific, the amplitude of CO_2 flux variability due to the ΔpCO_2 anomalies is decreased from 1958 to 2012 (Fig. 6d), consistent with the change in the relationship between wind speed and CO_2 fluxes. These results imply that anthropogenic forcing can further affect the relationship between factors determining the variability of CO_2 fluxes (wind speed and pCO_2) and itself in different regions. Next, the pronounced effect of wind speed on CO_2 fluxes is further illustrated by using a diagnostic analysis in the following.

3.4 The effects of wind speed and ΔpCO_2 on interdecadal variability of CO_2 fluxes: A diagnostic analysis

Wind speed has a vital influence on the gas transfer velocity, which further affects the air–sea CO_2 fluxes according to Eq. (2) (Wanninkhof and Triñanes 2017). In addition, the sign of CO_2 fluxes is determined by ΔpCO_2. To isolate the impacts of wind speed and ΔpCO_2 on CO_2 fluxes, analysis strategies are taken as follows:

(1) According to Eq. (1), the total wind fields (with seasonal to interdecadal signals all included) derived from the NCEP/NCAR, and other variables (ΔpCO_2, SST, SSS and DIC) derived from model output are used to calculate the CO_2 fluxes. This case is referred to as

Table 2 The mean values and standard deviations (trends) of various variables calculated during three different regimes (1958–1975, 1976–1997, and 1998–2012) and entire period (1958–2012)

	1958–1975	1976–1997	1998–2012	1958–2012
Tropical Pacific				
SST (°C decade^{-1}), °C	26.77 ± 0.21 (0.04)	26.99 ± 0.20 (− 0.06)	26.75 ± 0.20 (− 0.16)	26.86 ± 0.23 (0.005)
CO_2 flux (mol C m^2 year^{-1} decade^{-1}), mol C m^2 year^{-1}	1.07 ± 0.19 (− 0.04)	0.68 ± 0.14 (− 0.04)	0.76 ± 0.15 (0.02)	0.80 ± 0.26 (− 0.09)
pCO_2sea (ppm decade^{-1}), ppm	369.68 ± 7.05 (10.54)	388.77 ± 10.98 (14.76)	420.82 ± 9.21 (16.94)	393.52 ± 22.80 (12.82)
ΔpCO_2 (ppm decade^{-1}), ppm	47.87 ± 4.49 (1.51)	41.44 ± 5.54 (− 0.16)	41.54 ± 5.70 (− 3.92)	42.28 ± 7.67 (− 2.49)
Niño3 region				
SST (°C decade^{-1}), °C	25.50 ± 0.64 (0.28)	26.35 ± 0.69 (− 0.02)	26.10 ± 0.60 (− 0.17)	26.05 ± 0.76 (0.17)
CO_2 flux (mol C m^2 year^{-1} decade^{-1}), mol C m^2 year^{-1}	2.89 ± 0.68 (− 0.15)	1.87 ± 0.49 (− 0.00)	1.76 ± 0.36 (− 0.14)	2.11 ± 0.77 (− 0.29)
pCO_2sea (ppm decade^{-1}), ppm	448.47 ± 16.96 (10.81)	466.55 ± 24.39 (23.96)	498.06 ± 17.46 (7.61)	470.15 ± 27.79 (11.60)
ΔpCO_2 (ppm decade^{-1}), ppm	126.67 ± 16.08 (1.79)	119.22 ± 19.77 (9.05)	118.78 ± 17.82 (− 13.25)	118.91 ± 20.94 (− 3.71)
Niño4 region				
SST (°C decade^{-1}), °C	28.22 ± 0.55 (− 0.20)	28.66 ± 0.53 (− 0.02)	28.07 ± 0.62 (− 0.30)	28.37 ± 0.62 (− 0.02)
CO_2 flux (mol C m^2 year^{-1} decade^{-1}), mol C m^2 year^{-1}	1.40 ± 0.46 (0.40)	1.10 ± 0.36 (− 0.01)	1.56 ± 0.55 (0.23)	1.29 ± 0.51 (0.01)
pCO_2sea (ppm decade^{-1}), ppm	404.30 ± 19.47 (30.07)	421.85 ± 16.69 (14.76)	448.86 ± 16.64 (18.86)	427.81 ± 27.58 (13.27)
ΔpCO_2 (ppm decade^{-1}), ppm	82.50 ± 16.08 (21.04)	74.51 ± 14.58 (− 2.08)	79.28 ± 14.46 (− 2.60)	76.57 ± 16.83 (− 2.05)

Wind-inter, in which the effects of interannual variability of wind speed and ΔpCO_2 are both included.

(2) Then, the climatological field of wind speed is used to calculate the CO_2 fluxes (i.e. interannual-varying wind speed derived from the NCEP reanalysis is not taken into account). Other fields (ΔpCO_2, SST, SSS and DIC) are set the same as in Wind-inter. This case is referred to as Wind-clim, in which only seasonally varying wind speed is taken into account whereas interannual variability effect of ΔpCO_2 is included.

(3) Another analysis is conducted in which ΔpCO_2 is set to its climatology derived from model output, but wind speed is prescribed to be interannually varying as in Wind-inter. This case is referred to as ΔpCO_2-clim, i.e. interannual variability effect of ΔpCO_2 is excluded, whereas interannual variability of wind speed is retained.

Due to the quadratic dependence of gas transfer velocity (K_0) on wind speed (u) in Eq. 2, the interannual anomalies of wind speed directly amplify the interannual variability of K_0. Therefore, the interdecadal variability of gas transfer velocity K_0 (Eq. 2) can be directly linked to the frequency of El Niño and La Niña events during the IPO warm and cold phase. For example, during the IPO warm phase (1976–1997), El Niño events occur frequently (Fig. 4a), which leads to a decrease in wind speed in the central-eastern Pacific. Meanwhile, gas transfer velocity is assumed to be a quadratic dependency on wind speed (u^2) as described in Eq (2) (i.e. CO_2 fluxes $\propto u^2$), and so the effect of wind speed on CO_2 fluxes can be amplified through this quadratic dependency on interdecadal scale. Thus, an increase in the number of El Niño events can lead to a decrease in u^2, which subsequently leads to a decrease in CO_2 fluxes during the IPO warm phase.

Figure 7a–c shows the interdecadal anomalies of CO_2 fluxes derived from Wind-inter over three averaged periods (i.e. 1958–1975, 1976–1997, and 1998–2012). The maximum anomaly region of interdecadal CO_2 fluxes is located in the southeastern tropical Pacific, reaching 0.2 mol C m^{-2} year^{-1} during 1958–1975. The mean outgassing flux of CO_2 is 1.07 ± 0.19 mol C m^{-2} year^{-1} in the equatorial Pacific (18°S–18°N) during the period (Table 2), which is significantly higher than observational estimates during recent decades (Ishii et al., 2014). When the IPO phase becomes positive, the mean CO_2 fluxes decrease to 0.68 ± 0.14 mol C m^{-2} year^{-1} and interdecadal anomalies of CO_2 fluxes become negative in the entire equatorial Pacific during 1976–1997 (Table 2, Fig. 7b). In the recent period being so-called global warming "hiatus" (1998–2012), the rebound of overturning circulation may lead to an increase in the mean CO_2 fluxes (0.76 ± 0.15 mol C m^{-2} year^{-1}) (Table 2, Figs. 7c, 8a). It is noteworthy that the pattern of interdecadal anomalies of CO_2 fluxes exhibits the possible interaction between the tropics and extratropics. The pattern of interdecadal anomalies in CO_2 fluxes is similar to the paths of water parcels as suggested by Gu and Philander (1997) and Zhang et al. (1998).

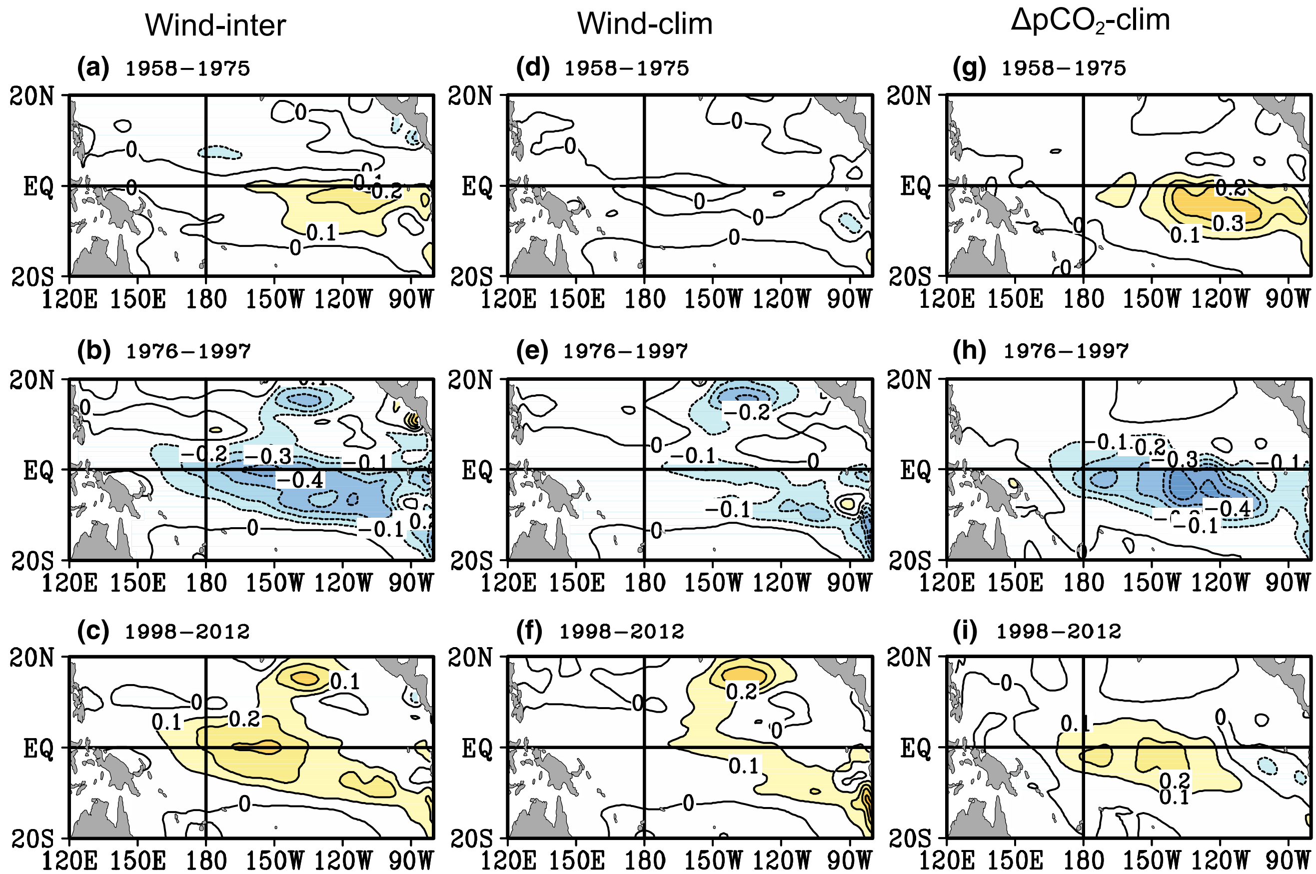

Fig. 7 The detrended interdecadal anomalies of CO_2 fluxes during the period of 1958–1975 (**a**), 1976–1997 (**b**) and 1998–2012 (**c**), which are calculated using interannually varying wind (denoted as Wind-inter). The **d**–**f** and **g**–**i** are the same as in **a**–**c** but for the results derived using climatological winds (denoted as Wind-clim) and climatological ΔpCO_2 (denoted as ΔpCO_2-clim), respectively. The contour intervals are 0.1 mol C m^{-2} $year^{-1}$

In the Wind-clim case, the effect of interdecadal wind of variability is removed in the calculation of CO_2 fluxes. The resultant amplitude of interdecadal variability in CO_2 fluxes is significantly weakened in the western-central equatorial Pacific (Figs. 7d–f, 8c). The weakened interdecadal variability of CO_2 fluxes in Wind-clim indicates that interdecadal variability of wind speed plays a dominant role in determining the amplitude and location of interdecadal variability of CO_2 fluxes. In Fig. 7a–c, the region with maximum interdecadal anomalies of CO_2 fluxes gradually migrates westward along the equator in Wind-inter, but this feature is not evident in Wind-clim. As shown in Fig. 4b, the region with large interannual and interdecadal variabilities of wind speed tends to be confined to the central equatorial Pacific. In Wind-clim, the effects of interannual and interdecadal variability of wind speed are excluded, so the interdecadal anomalies of CO_2 fluxes are mainly due to the change in ΔpCO_2. Figure 7d–f show that the impacts of ΔpCO_2 on CO_2 fluxes are mainly located in the northern tropical ocean and southeastern Pacific on interdecadal timescale, indicating that the effects of ΔpCO_2 on CO_2 fluxes come from the off-equatorial region.

Figure 7g–i show interdecadal anomalies of CO_2 fluxes in the ΔpCO_2-clim. In this case, the effect from interannual and interdecadal variability of ΔpCO_2 is excluded. This result can be compared to that of Wind-inter in terms of the amplitude and location of interdecadal CO_2 flux anomalies. In ΔpCO_2-clim, the amplitudes of interdecadal variability in CO_2 fluxes are slightly weakened in the western-central equatorial Pacific as indicated in Fig. 7g–i, indicating that the impact of wind speed dominates interdecadal variability of CO_2 fluxes, whereas that of ΔpCO_2 plays a secondary role in determining the interdecadal variability of CO_2 fluxes. In addition, the interannual variability of wind speed is more important on that of CO_2 fluxes in the central Pacific, while that of ΔpCO_2 is important in the eastern Pacific and extratropics (Figs. 7d–f, 8b). Overall, wind speed plays a vital role in determining the interdecadal variability of CO_2 fluxes, and the contribution from ΔpCO_2 is relatively small.

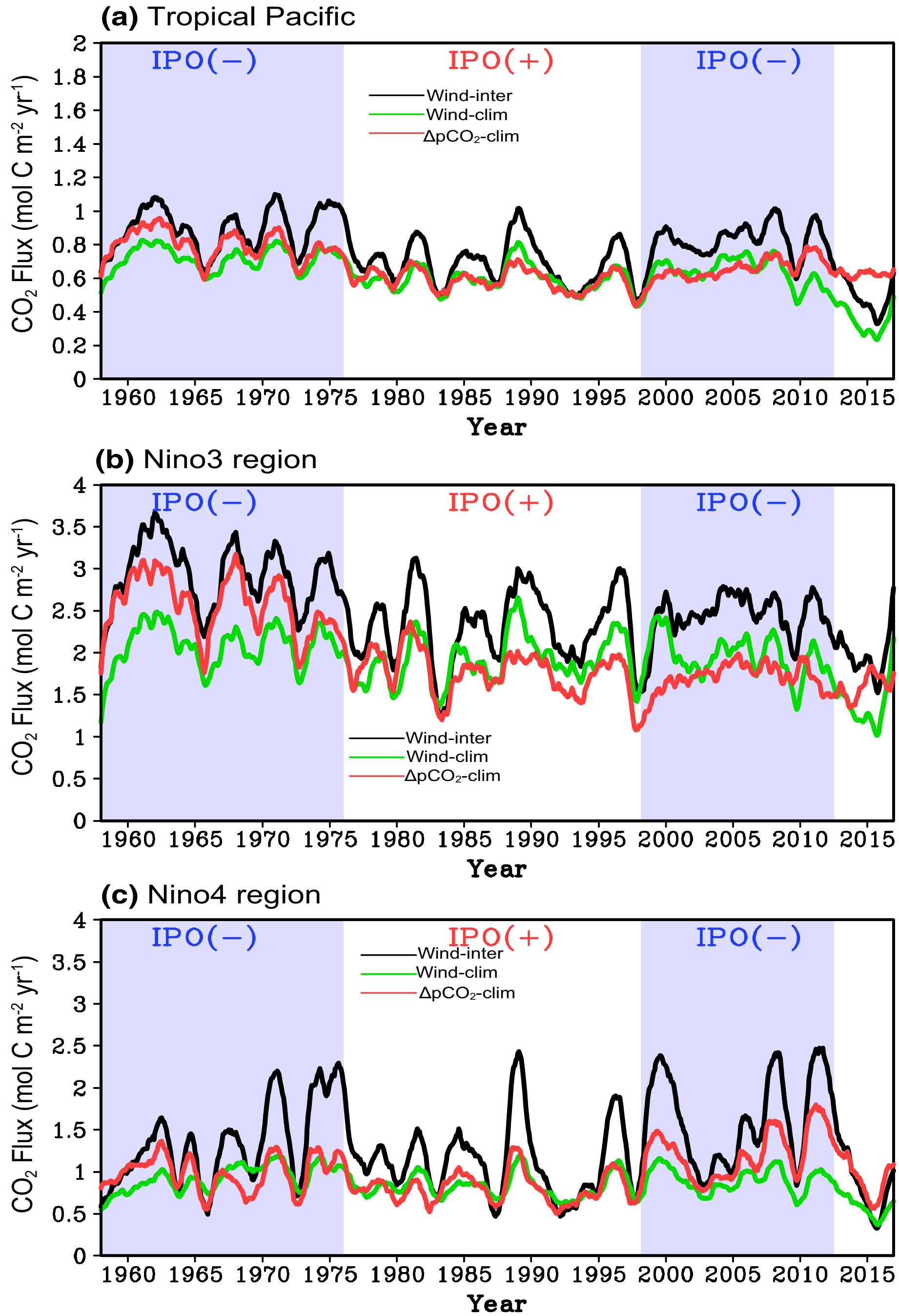

Fig. 8 Mean fields of air–sea CO_2 fluxes diagnosed from Wind-inter (black line), Wind-clim (green line) and ΔpCO_2-clim (red line) during 1958-2016 for the entire tropical Pacific (18°S–18°N) (**a**), the Niño3 region (**b**) and the Niño4 region (**c**), respectively. The results are shown for smoothed values with 13-month running mean

3.5 Interdecadal variability of sea surface pCO_2

The ΔpCO_2 (surface water pCO_2 minus atmospheric pCO_2) is another major factor in determining the outgassing of CO_2 into the atmosphere (Eq. 2), especially in terms of determining the sign of CO_2 fluxes at the air–sea interface. Although the contribution of ΔpCO_2 to CO_2 fluxes is relatively small in the tropical Pacific (Fig. 8), the interdecadal change of ΔpCO_2 is still evident in some regions (Figs. 3, 4). The interdecadal variability of ΔpCO_2 and the mechanism responsible for it are analyzed in this section.

Due to the effect of anthropogenic activity, global atmospheric pCO_2 has been continuously increasing from 1948 (315 ppm) to 2017 (406 ppm) (https://www.esrl.noaa.gov/gmd/ccgg/trends/full.html) (Fig. 9; blue line). Therefore, interdecadal change of ΔpCO_2 is mainly attributed to variability of sea surface pCO_2. Observational records of ocean surface pCO_2 in the central equatorial Pacific show that sea surface pCO_2 increased at a similar rate to the atmospheric CO_2, which leads to zero trend in ΔpCO_2 since 1980s (DiNezio et al. 2015). The modeled results are consistent with observational records, and

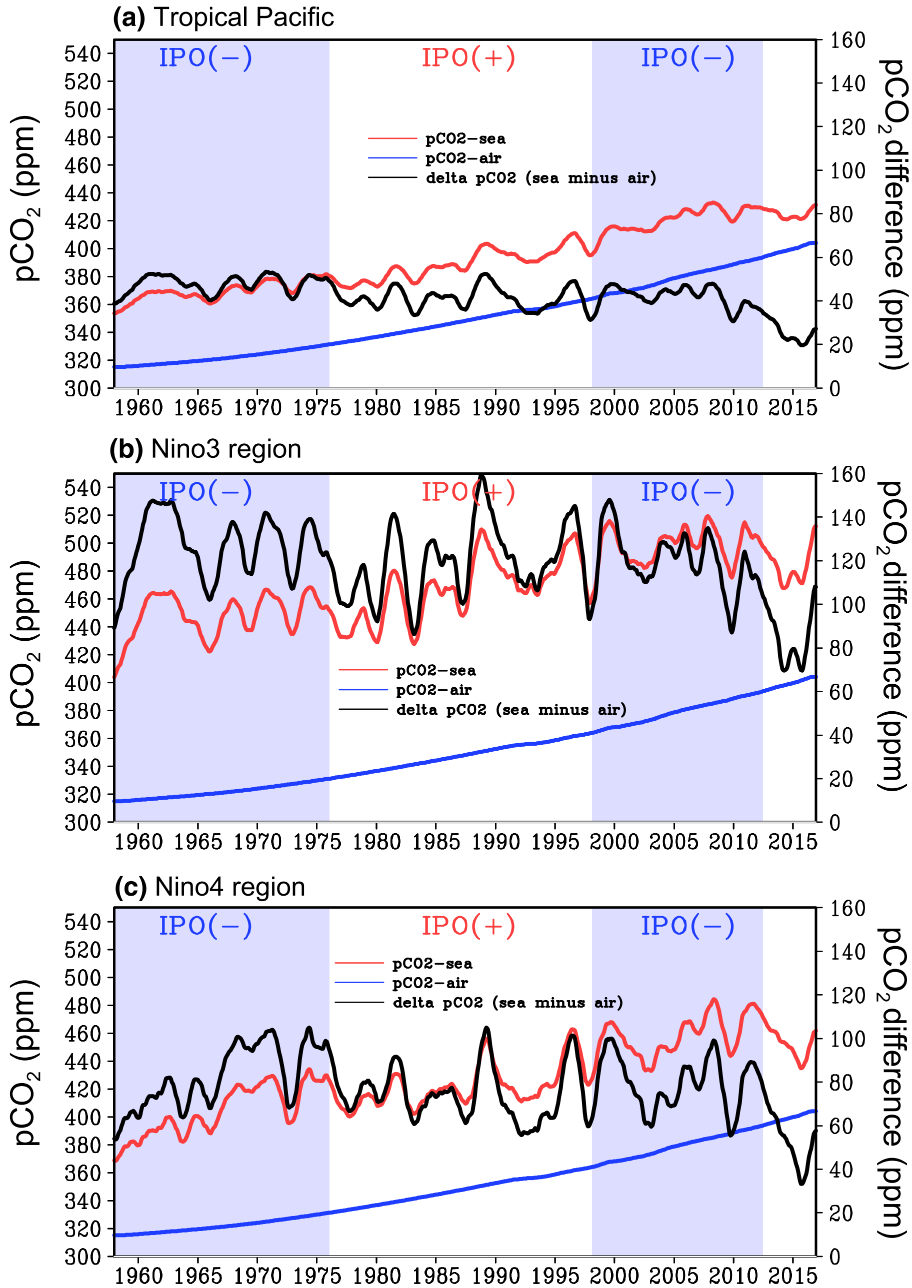

Fig. 9 Mean fields of sea surface pCO_2, atmospheric pCO_2 and ΔpCO_2 during 1958–2016 for the entire tropical Pacific (18°S–18°N) (**a**), Niño3 region (**b**) and Niño4 region (**c**). The results are shown for smoothed values with 13-month running mean

ΔpCO_2 appears to be zero-trend during the last two periods in the tropical Pacific (41.44 ppm during 1976–1997, 41.54 ppm 1998–2012) (Table 2, Fig. 9a). The near-zero change of ΔpCO_2 is strikingly evident in the Niño3 region (119.22 ppm during 1976–1997, 118.78 ppm 1998–2012) (Fig. 9b and Table 2). In addition, the results from the fifth phase of the Coupled Model Intercomparison Project (CMIP5) and large member ensemble of simulations from CESM show a decrease trend in ΔpCO_2 during the period of 2030–2070 when atmospheric CO_2 increases (DiNezio et al. 2015). Therefore, the nearly zero trend of ΔpCO_2 indicates that interdecadal variability of sea surface pCO_2 may mask the anthropogenic forcing induced change on long-term trend of ΔpCO_2 in the tropical Pacific.

However, in the Niño4 region, interdecadal variability of ΔpCO_2 is still obvious (74.51 ppm during 1976–1997, 79.28 ppm 1998–2012) (Table 2, Fig. 9c). Meanwhile, large interdecadal variability of wind speed is also located in the Niño4 region (Fig. 4b). Thus, the combined effects of both wind speed and ΔpCO_2 act to strengthen interdecadal variability of CO_2 fluxes in the western-central equatorial Pacific. In the Niño3 region, the changes of ΔpCO_2 during the last two periods are very small. This relatively small change in ΔpCO_2 partially can explain why the contribution of ΔpCO_2 to CO_2 fluxes is small in the eastern equatorial Pacific (Table 2).

3.5.1 A component analysis of sea surface pCO_2

Figure 9 shows that interdecadal ΔpCO_2 variability is mainly determined by variability of pCO_2 at sea surface (Eq. 1), which is influenced by DIC, SST, SSS and alkalinity. To assess the relative contributions of different components, we conducted a component analysis developed by Takahashi et al. (1993) as follows (Eq. 3),

$$\frac{dpCO_2}{dt} = \frac{\partial pCO_2}{\partial DIC}\frac{dDIC}{dt} + \frac{\partial pCO_2}{\partial T}\frac{dT}{dt} + \frac{\partial pCO_2}{\partial ALK}\frac{dALK}{dt} + \frac{\partial pCO_2}{\partial S}\frac{dS}{dt} \tag{3}$$

where pCO_2 is sea surface partial pressure of CO_2; DIC is concentration of dissolved inorganic carbon within the mixed layer; T is sea surface temperature; ALK is total alkalinity and S is sea surface salinity. According to Table 8.3.1 in Sarmiento and Gruber (2006), we take

$$\frac{1}{pCO_2}\frac{\partial pCO_2}{\partial T} = 0.0423\ ^\circ C^{-1}$$

$$\frac{S}{pCO_2}\frac{\partial pCO_2}{\partial S} = 1$$

$$\frac{ALK}{pCO_2}\frac{\partial pCO_2}{\partial ALK} = -8.9$$

$$\frac{DIC}{pCO_2}\frac{\partial pCO_2}{\partial DIC} = 9.5$$

Figure 10 shows that sea surface pCO_2 exhibits pronounced interdecadal variability; i.e. sea surface pCO_2 increases during the cold phase (1958–1975, 1998–2012), but decreases during the warm phase (1976–1997) of the IPO (Fig. 10). The contribution due to SST is out of phase with that due to DIC, indicating that the contributions from SST and DIC tend to cancel out each other on interdecadal timescale, whereas the contributions due to salinity and alkalinity effects to sea surface pCO_2 are small. During the IPO positive phase, an increase in SST leads to an increase in seawater pCO_2 due to thermodynamics (Fig. 3b, black dash line). In contrast, weak upwelling and vertical mixing during this warm phase of the IPO bring the subsurface water with lower DIC into the upper layer, acting to decrease the seawater pCO_2. During the cold phase of the IPO (1958–1975, 1998–2012), an increase in trade winds leads to an enhanced upwelling and vertical mixing, which leads to a decrease in SST and an increase in DIC. Nevertheless, a decrease in SST acts to reduce solubility of CO_2 in the seawater, which tends to decrease the sea surface pCO_2. As shown in Fig. 10, the change of sea surface pCO_2 is in phase with that of DIC but out of phase with that of SST, indicating that DIC plays a dominant role in determining interdecadal variability of sea surface pCO_2. Additionally, the change of $\frac{dpCO_2}{dt}$ is slightly larger in the Niño4 region than that in the Niño3 region, suggesting that interdecadal change of sea surface pCO_2 is stronger in the central equatorial Pacific.

3.5.2 Mixed layer DIC budget analysis: physical vs. biological processes

Based on the dominant effect of DIC on the sea surface pCO_2 on interdecadal timescale, we also analyzed the DIC budget within the mixed layer. Related analyses have been conducted by previous studies on interannual to decadal

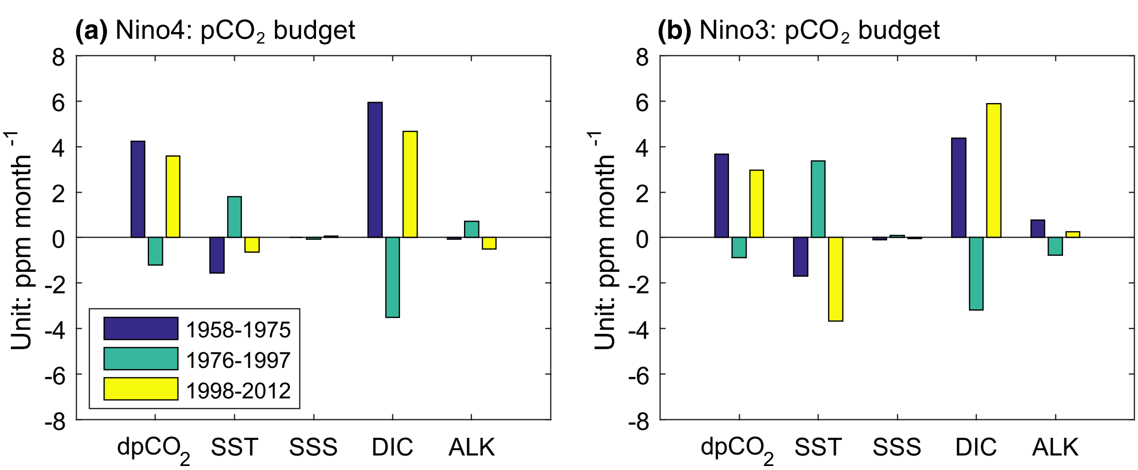

Fig. 10 Component analyses of sea surface pCO_2 in the Niño4 region (**a**) and the Niño3 region (**b**). All variables are calculated over the three different periods (1958–1975, 1976–1997, and 1998–2012)

timescales (Wang et al. 2006, 2015). The DIC budget within the mixed layer can be written as

$$\frac{\partial C}{\partial t} = -u\frac{\partial C}{\partial x} - v\frac{\partial C}{\partial y} - w\frac{\partial C}{\partial z} + C_{mix} - NCP - \frac{FCO_2}{h} \quad (4)$$

where C represents DIC concentration in the mixed layer; u, v, w are the zonal, meridional and vertical velocity, respectively; C_{mix} is vertical mixing and entrainment terms (the sum of mixing and advection terms are called physical term); NCP represents the biological process (including uptake and regeneration); FCO_2 is air–sea exchange of CO_2, i.e. CO_2 fluxes (h is the mixed layer depth).

Figure 11a shows large interannual and interdecadal variabilities of DIC in the central-eastern equatorial Pacific. Due to the close relationship between La Niña (El Niño) activities and cold (warm) phases of the IPO (Lin et al. 2018; An 2018), frequencies of El Niño and La Niña events occurring can directly influence the variations of DIC on interdecadal timescale. For example, during the cold phase of the IPO, thermocline depth is shallow, which favors the occurring of La Niña events. Meanwhile, during La Niña events, the equatorial upwelling is enhanced, which consequently leads to an increase in DIC concentration in the eastern equatorial Pacific.

Figure 12a, b show that ocean dynamic processes (including advection and mixing) dominate the interdecadal variability of DIC. The ocean dynamic processes lead to an increase in DIC during the cold phase of the IPO (1958–1975, 1998–2012), and a decrease during the warm phase of the IPO (1976–1997), especially in the central Pacific. This result indicates that DIC experiences interdecadal fluctuations in the central equatorial Pacific. Additionally, in the central Pacific, the contributions of each components (physical process, biological uptake and gas exchange) to DIC are gradually increased in these three periods, and interdecadal signals of these components are still evident (Fig. 12a). Overall, interdecadal signals of DIC overwhelm the long-term trend in the western-central Pacific.

However, in the eastern Pacific, the contributions of each components to DIC interdecadal change are reduced during these three sub-periods (Fig. 12b). During the last two periods (1976–1997 and 1998–2012), contributions from physical dynamic term and biological uptake in DIC show nearly

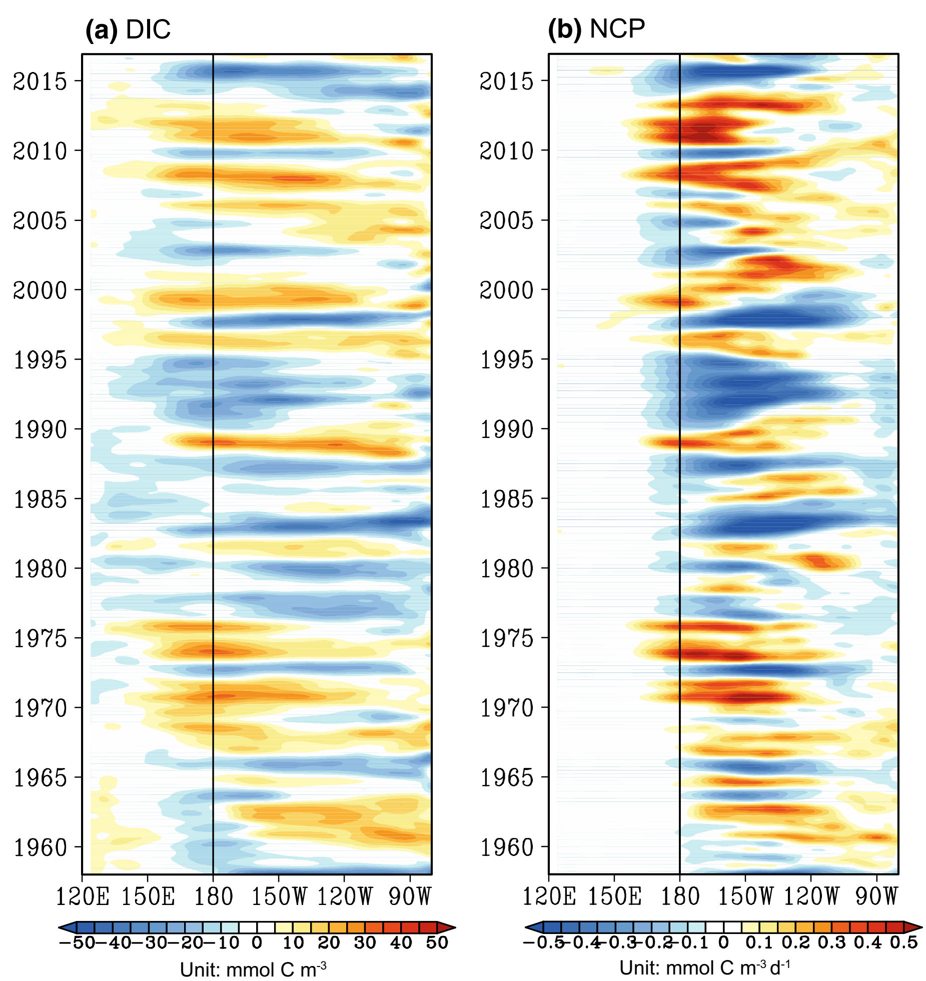

Fig. 11 The interannual anomalies along the equator for DIC (**a**) and NCP (**b**) within the mixed layer during the period 1958–2016. The long-term trends are removed. The units are mmol C m^{-3} in **a** and mmol C m^{-3} $days^{-1}$ in **b**

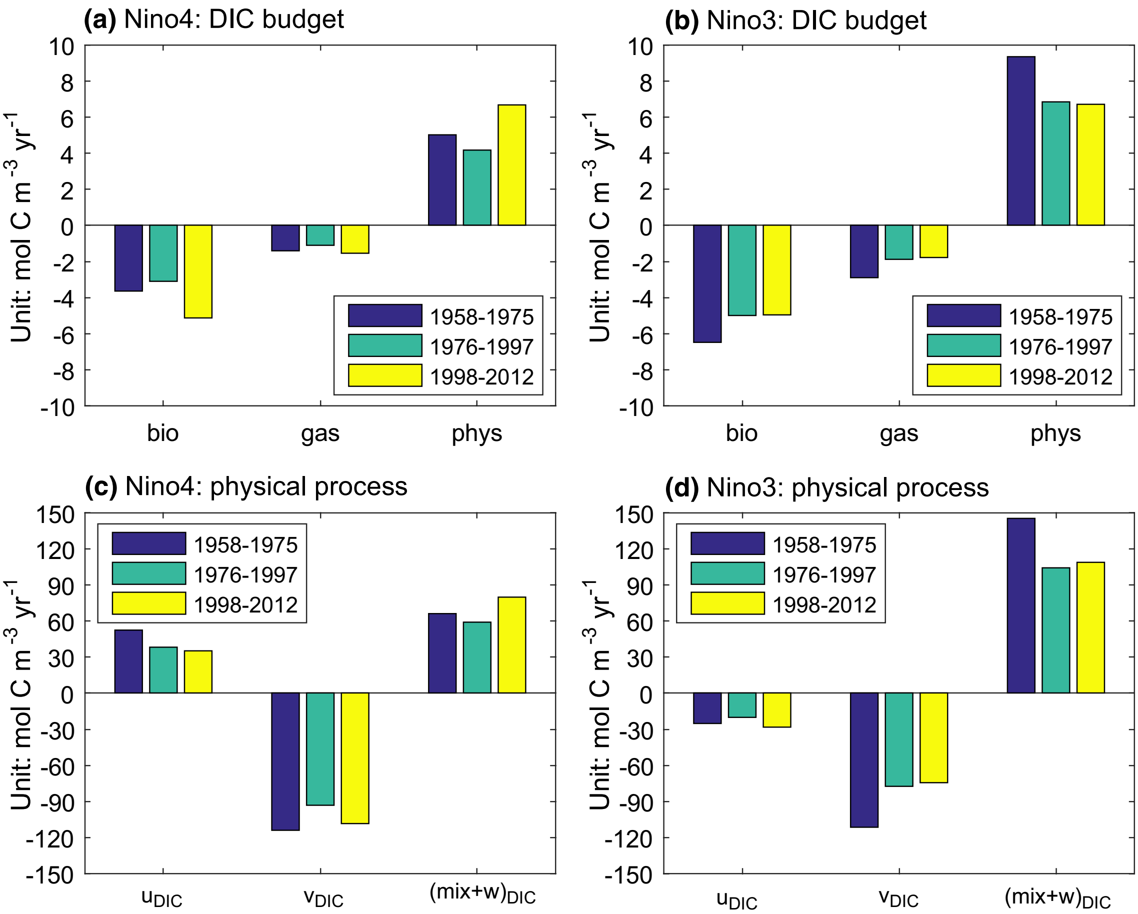

Fig. 12 Budget analyses of DIC in the Niño4 region (**a**) and the Niño3 region (**b**). The contributions of physical processes, which are divided into zonal advevction (denoted as u_{DIC}), meridional advection (denoted as v_{DIC}), and mixing and vertical advection [denoted as $(mix + w)_{DIC}$], are shown for the Niño4 region (**c**) and Niño3 region (**d**), respectively. All variables are calculated over three different periods (1958–1975, 1976–1997, and 1998–2012), respectively. The units are mol C m^{-3} $year^{-1}$

zero change (Fig. 12b). For example, the contributions of the physical processes keep on hold in the Niño3 region. This is because an increase in upwelling during cold phase of the IPO is compensated for by the decrease in upwelling during long-term trend period induced by the global warming (Collins et al. 2010). These processes in turn modulate relative contributions of each components to long-trend of DIC in the eastern equatorial Pacific.

The biological process and air–sea gas exchange play vital roles in balancing physical processes in the DIC budget; the biological process removes most of DIC due to biological uptake and regeneration (Fig. 12a, b). Meanwhile, Fig. 11b shows a strong interannual variability of NCP, with large variability being located in the central equatorial Pacific, which is similar to that of CO_2 fluxes. Biological uptake is tightly associated with biological activity, and exhibits a decreased trend during the twentieth century (Boyce et al. 2010). In addition, phytoplankton biomass exhibits an increased trend in the tropical Pacific during the recent 20 years (Sharma et al. 2019). The combined effects of long-term trend and interdecadal change in biological uptake contribute to a zero-change of DIC during the last two periods in the eastern Pacific (Fig. 12b).

Due to the dominant roles played by physical processes in interdecadal variability of DIC, these terms (zonal, meridional advection, and the vertical mixing and advection terms of DIC) in the Niño3 and Niño4 region are shown separately in Fig. 12c, d. In the central equatorial Pacific (Fig. 12c), zonal DIC advection and vertical mixing of DIC tend to be compensated for meridional DIC advection, with their net differences being dominated by contributions of physical processes in Fig. 12a. Noteworthy, the meridional advection is stronger than vertical mixing and zonal advection, and exhibits clear interdecadal fluctuations in the Niño4 region.

In the eastern equatorial Pacific (Fig. 12d), vertical mixing dominates interdecadal variability of DIC and overwhelms the sum of zonal and meridional advection. Moreover, the interdecadal change in physical term of DIC budget exhibits a near-zero trend during the last two periods (1976–1997 and 1998–2012), which may be the reason why the change of ΔpCO_2 is very small in the eastern equatorial Pacific. Overall, in responses to the regime shift of the IPO, the change in dynamical process affects the interdecadal variability of DIC, with its effects on DIC being most significant in the central equatorial Pacific. Consequently, the remarkable interdecadal change of DIC contributes to that of sea surface pCO_2 in the central equatorial Pacific.

4 Discussion

CO_2 fluxes are mainly determined by atmospheric wind speed and ΔpCO_2 at the air–sea interface. On one hand, because the wind speed exhibits quadratic dependence on gas transfer velocity, it can influence the magnitude of CO_2 fluxes. On the other hand, the sign of CO_2 fluxes is determined by ΔpCO_2. Therefore, ΔpCO_2 is the factor that determines whether the ocean is a source or sinks for CO_2, while wind speed can amplify or reduce the magnitude of releasing or absorbing CO_2 at the sea surface. At present, how CO_2 fluxes are affected by these two factors and their relative contributions on interdecadal timescale have not been understood well.

In this study, a modeling study and corresponding analysis are performed. Two apparent regime shifts of air–sea CO_2 fluxes in the tropical Pacific are found in 1975–1976 and 1997–1998, which are associated with the regime shift of the IPO (Chen and Tung 2018). Since 2000s, a La Niña-like cooling associated with the cold phase of the IPO emerges in the eastern tropical Pacific; this period is often called global warming hiatus (Kosaka and Xie 2013). However, a possible ending of global warming hiatus occurred during 2014–2016 (Hu and Fedorov 2017). Meanwhile, a sharp decline of ΔpCO_2 by 20 ppm is remarkable in Fig. 9 during 2014–2016. This is because sea surface pCO_2 exhibits little change during 2012–2016, but atmospheric pCO_2 (pCO_{2air}) continuously rises due to anthropogenic activity. As discussed in Hu and Fedorov (2017), the possible ending of global warming hiatus may be linked to the phase change in the IPO from its cold phase to warm phase. During the warm phase of the IPO, weakened trade winds and upwelling can result in a decrease in DIC and ΔpCO_2. In addition, under global warming scenario, weakened trade winds also lead to a weakening of the equatorial upwelling, causing reductions in DIC and ΔpCO_2. Thus, a decrease in ΔpCO_2 due to the warm phase of the IPO is superimposed onto a decline trend of seawater ΔpCO_2 due to global warming, which may further reduce the ΔpCO_2 in the next warm phase of the IPO. Consequently, the decrease in ΔpCO_2 and wind speed due to global warming may lead to a reduction of CO_2 fluxes in the next several decades. In the north Pacific subtropical gyre, Sutton et al. (2017) found that warm anomalies drove elevated seawater pCO_2, and caused this region to be a net CO_2 source for the first time in the observational records. They further suggested that climatic forcing could influence the timing of regional oceanic shift from a sink to a source. Whether the sign of ΔpCO_2 can be changed from positive to negative in some region is important to the carbon cycle in the tropical Pacific, which should be investigated in the future.

Gu and Philander (1997) found that the link between the tropics and the extratropics (whose effects are rapid and poleward in the atmosphere but slow and equatorward in the oceans) can cause the interdecadal fluctuation in the Pacific. Zhang et al. (1998) presented observational evidence for decadal changes in ENSO that may originate from mid-latitude decadal variability. In this study, clear links between the tropics and the extratropics are found in the interdecadal anomalies of CO_2 fluxes (Fig. 7). Recent studies show that the reemergence of anthropogenic CO_2 through the recirculation within the subtropical cells can lead to the reduction of CO_2 uptake in the surface ocean, which can potentially induce a positive climate-carbon feedback (Zhai et al. 2017). The interaction between the tropics and extratropics on interdecadal variability of CO_2 fluxes should be investigated in the future.

In addition, the choice of wind speed products can exert significant influence on the calculation of CO_2 fluxes. In this study, we only employ wind products from the NCEP/NCAR reanalysis to calculate the CO_2 fluxes, but the uncertainty in wind fields can induce 30–37% change of CO_2 fluxes in the mean global ocean carbon uptake (Roobaert et al. 2018). For projection on future interdecadal variability of CO_2 fluxes, the accuracy of wind speed projection can significantly affect the global carbon cycle and even further climate change. Also, the results are obtained from a layer model; other level ocean models need to be used to perform similar experiments (e.g. Kang et al. 2017).

5 Summary

It is well recognized that the equatorial Pacific is the largest natural source region for CO_2 fluxes, which accounts for 70% interannual variability of global CO_2 fluxes. However, the interdecadal variability of CO_2 fluxes in this region has not been understood well. Here, we examine the interdecadal variability of CO_2 fluxes by using a coupled ocean physics–biogeochemical model forced by prescribed wind from NCEP/NCAR reanalysis during 1948–2016. Two regime shifts are found in 1975–1976 and 1997–1998, which are consistent with the phase transitions of the interdecadal Pacific Oscillation (IPO). Modelling results indicate that the ΔpCO_2 has a near-zero trend in the recent two phases

(1976–1997 and 1998–2012), which are related to the global warming hiatus. However, the rebound of CO_2 fluxes in recent decades (1998–2012) is mainly determined by the increase in wind speed. Additionally, one major finding from this study is that the large interdecadal variability region of CO_2 fluxes is concentrated on in the central equatorial Pacific. The relationships between CO_2 fluxes and wind speed variability indicate that their interdecadal fluctuations are mostly pronounced in the central-western tropical Pacific, but not in the eastern Pacific. Overall, the interdecadal variability of wind speed plays a key role in determining that of CO_2 fluxes. The contribution from the ΔpCO_2 to interdecadal variability of CO_2 fluxes is relatively small.

The interdecadal variability of CO_2 fluxes can partly mask the decreased trend in outgassing CO_2 in the equatorial Pacific and further increase the uncertainty in projection on ocean sink for anthropogenic CO_2, which in turn has a significant influence on the atmospheric CO_2 level. Due to the importance of the equatorial Pacific in the global carbon cycle, interdecadal fluctuations of CO_2 fluxes may exert a significant influence on the carbon sink of global ocean under the scenario of global warming. These relationships need to be investigated in the near future.

Acknowledgements The authors wish to thank the anonymous reviewers and editor for their insightful comments that greatly helped to improve the original manuscript. We would like to thank Zeng-Zhen Hu, Jieshun Zhu, Zhaohua Wu for their comments. This research was supported by the National Natural Science Foundation of China (NFSC; Grant nos. 41475101, 41690122(41690120), 41490644(41490640), 41421005), the Strategic Priority Research Program of the Chinese Academy of Sciences (Grant no. XDA19060102), the NSFC-Shandong Joint Fund for Marine Science Research Centers (U1406402), and Taishan Scholarship. The data and computer codes used in the paper are available from the authors (e-mail: rzhang@qdio.ac.cn).

References

An S-I (2018) Impact of Pacific decadal oscillation on frequency asymmetry of El Niño and La Niña Events. Adv Atmos Sci 35:493–494. https://doi.org/10.1007/s00376-018-8024-7

Ashok K, Yamagata T (2009) Climate change: the El Niño with a difference. Nature 461:481–484. https://doi.org/10.1038/461481a

Bakker DCE, Pfeil B, Landa CS et al (2016) A multi-decade record of high-quality fCO2 data in version 3 of the surface ocean CO2 Atlas (SOCAT). Earth Syst Sci Data 8:383–413. https://doi.org/10.5194/essd-8-383-2016

Bordbar MH, Martin T, Latif M, Park W (2017) Role of internal variability in recent decadal to multidecadal tropical Pacific climate changes. Geophys Res Lett 44:4246–4255. https://doi.org/10.1002/2016GL072355

Boyce DG, Lewis MR, Worm B (2010) Global phytoplankton decline over the past century. Nature 466:591–596. https://doi.org/10.1038/nature09268

Chen X, Tung K-K (2018) Global-mean surface temperature variability: space–time perspective from rotated EOFs. Clim Dyn 51:1719–1732. https://doi.org/10.1007/s00382-017-3979-0

Chen D, Rothstein LM, Busalacchi AJ (1994) A hybrid vertical mixing scheme and its application to tropical ocean models. J Phys Oceanogr 24:2156–2179. https://doi.org/10.1175/1520-0485(1994)024%3c2156:AHVMSA%3e2.0.CO;2

Choi J, Il An S, Yeh SW (2012) Decadal amplitude modulation of two types of ENSO and its relationship with the mean state. Clim Dyn 38:2631–2644. https://doi.org/10.1007/s00382-011-1186-y

Collins M, An S-I, Cai W et al (2010) The impact of global warming on the tropical Pacific Ocean and El Niño. Nat Geosci 3:391–397. https://doi.org/10.1038/ngeo868

DiNezio PN, Barbero L, Long MC et al (2015) Are anthropogenic changes in the tropical ocean carbon cycle being masked by Pacific decadal variability? US CLIVAR 13:12–16

Doney SC, Tilbrook B, Roy S et al (2009) Surface-ocean CO2 variability and vulnerability. Deep Res Part II Top Stud Oceanogr 56:504–511. https://doi.org/10.1016/j.dsr2.2008.12.016

Dunne JP, Laufkötter C, Frölicher TL (2015) Ocean biogeochemistry in the fifth coupled model intercomparison project (CMIP5). CLIVAR Newsl 13:1–29

England MH, McGregor S, Spence P et al (2014) Recent intensification of wind-driven circulation in the Pacific and the ongoing warming hiatus. Nat Clim Chang 4:222–227. https://doi.org/10.1038/NCLIMATE2106

Fay AR, McKinley GA (2013) Global trends in surface ocean pCO2 from in situ data. Global Biogeochem Cycles 27:541–557. https://doi.org/10.1002/gbc.20051

Feely RA, Wanninkhof R, Takahashi T, Tans P (1999) Influence of El Niño on the equatorial Pacific contribution to atmospheric CO2 accumulation. Nature 398:597. https://doi.org/10.1038/19273

Feely RA, Takahashi T, Wanninkhof R et al (2006) Decadal variability of the air–sea CO2 fluxes in the equatorial Pacific Ocean. J Geophys Res 111:C08S90. https://doi.org/10.1029/2005jc003129

Gent PR, Cane MA (1989) A reduced gravity, primitive equation model of the upper equatorial ocean. J Comput Phys 81:444–480. https://doi.org/10.1016/0021-9991(89)90216-7

Gu D, Philander SGH (1997) Interdecade climate fluctuations that depend on exchanges between the tropic and extratropics. Science (80-) 275:805–807

Han W, Meehl GA, Hu A et al (2014) Intensification of decadal and multi-decadal sea level variability in the western tropical Pacific during recent decades. Clim Dyn 43:1357–1379. https://doi.org/10.1007/s00382-013-1951-1

Hu S, Fedorov AV (2017) The extreme El Niño of 2015–2016 and the end of global warming hiatus. Geophys Res Lett 44:3816–3824. https://doi.org/10.1002/2017GL072908

Huang B, Thorne PW, Banzon VF et al (2017) Extended reconstructed sea surface temperature version 5 (ERSSTv5): upgrades, validations, and intercomparisons. J Clim 5:8179–8205. https://doi.org/10.1175/jcli-d-16-0836.1

Ishii M, Inoue HY, Midorikawa T et al (2009) Spatial variability and decadal trend of the oceanic CO2 in the western equatorial Pacific warm/fresh water. Deep Res Part II Top Stud Oceanogr 56:591–606. https://doi.org/10.1016/j.dsr2.2009.01.002

Ishii M, Feely RA, Rodgers KB et al (2014) Air-sea CO2 flux in the Pacific Ocean for the period 1990–2009. Biogeosciences 11:709–734. https://doi.org/10.5194/bg-11-709-2014

Kalnay E, Kanamitsu M, Kistler R et al (1996) The NCEP/NCAR 40-year reanalysis project. Bull Am Meteorol Soc 77:437–471. https://doi.org/10.1175/1520-0477(1996)077%3c0437:TNYRP%3e2.0.CO;2

Kang X, Zhang R-H, Wang G (2017) Effects of different freshwater flux representations in an ocean general circulation model of the tropical Pacific. Sci Bull 62:345–351. https://doi.org/10.1016/j.scib.2017.02.002

Kosaka Y, Xie S-P (2013) Recent global-warming hiatus tied to equatorial Pacific surface cooling. Nature 501:403–407. https://doi.org/10.1038/nature12534

Kug J-S, Jin F-F, An S-I (2009) Two types of El Niño events: cold tongue El Niño and warm Pool El Niño. J Clim 22:1499–1515. https://doi.org/10.1175/2008JCLI2624.1

Landschützer P, Gruber N, Bakker DCE, Schuster U (2014) Recent variability of the global ocean carbon sink. Global Biogeochem Cycles 28:927–949. https://doi.org/10.1002/2014GB004853

Landschützer P, Gruber N, Bakker DCE (2016) Decadal variations and trends of the global ocean carbon sink. Global Biogeochem Cycles 30:1396–1417. https://doi.org/10.1002/2015GB005359

Le Quéré C, Orr JC, Monfray P et al (2000) Interannual variability of the oceanic sink of CO2 from 1979 through 1997. Global Biogeochem Cycles 14:1247–1265. https://doi.org/10.1029/1999GB900049

Lin R, Zheng F, Dong X (2018) ENSO frequency asymmetry and the Pacific decadal oscillation in observations and 19 CMIP5 models. Adv Atmos Sci 35:495–506. https://doi.org/10.1007/s00376-017-7133-z

Liu Z (2012) Dynamics of interdecadal climate variability: a historical perspective*. J Clim 25:1963–1995. https://doi.org/10.1175/2011JCLI3980.1

Mantua NJ, Hare SR, Zhang Y et al (1997) A Pacific interdecadal climate oscillation with impacts on salmon production. Bull Am Meteorol Soc 78:1069–1079. https://doi.org/10.1175/1520-0477(1997)078%3c1069:APICOW%3e2.0.CO;2

McKinley GA, Fay AR, Lovenduski NS, Pilcher DJ (2017) Natural variability and anthropogenic trends in the ocean carbon sink. Ann Rev Mar Sci 9:125–150. https://doi.org/10.1146/annurev-marine-010816-060529

McPhaden MJ, Zhang D (2002) Slowdown of the meridional overturning circulation in the upper Pacific Ocean. Nature 415:603–608. https://doi.org/10.1038/415603a

Meehl GA, Hu A, Teng H (2016) Initialized decadal prediction for transition to positive phase of the Interdecadal Pacific Oscillation. Nat Commun 7:1–7. https://doi.org/10.1038/ncomms11718

Murtugudde R, Seager R, Busalacchi A (1996) Simulation of the tropical oceans with an ocean GCM coupled to an atmospheric mixed-layer model. J Clim 9:1795–1815. https://doi.org/10.1175/1520-0442(1996)009%3c1795:SOTTOW%3e2.0.CO;2

Newman M, Compo GP, Alexander MA (2003) ENSO-forced variability of the Pacific decadal oscillation. J Clim 16:3853–3857. https://doi.org/10.1175/1520-0442(2003)016%3c3853:EVOTPD%3e2.0.CO;2

Patra PK, Maksyutov S, Ishizawa M et al (2005) Interannual and decadal changes in the sea-air CO2 flux from atmospheric CO2 inverse modeling. Global Biogeochem Cycles. https://doi.org/10.1029/2004gb002257

Power S, Casey T, Folland C et al (1999) Inter-decadal modulation of the impact of ENSO on Australia. Clim Dyn 15:319–324. https://doi.org/10.1007/s003820050284

Rayner PJ, Law RM, Dargaville R (1999) The relationship between tropical CO2 fluxes and the El Niño-Southern Oscillation. Geophys Res Lett 26:493–496. https://doi.org/10.1029/1999GL900008

Roobaert A, Laruelle GG, Landschützer P, Regnier P (2018) Uncertainty in the global oceanic CO2 uptake induced by wind forcing: quantification and spatial analysis. Biogeosciences 15:1701–1720. https://doi.org/10.5194/bg-15-1701-2018

Sarmiento JL, Gruber N (2006) Ocean biogeochemical dynamics. Pricenton University Press, Princeton

Seager R, Blumenthal MB, Kushnir Y (1995) An advective atmospheric mixed layer model for ocean modeling purposes: global simulation of surface heat fluxes. J Clim 8:1951–1964. https://doi.org/10.1175/1520-0442(1995)008%3c1951:AAAMLM%3e2.0.CO;2

Sharma P, Marinov I, Cabre A et al (2019) Increasing biomass in the warm oceans: unexpected new insights from SeaWiFS. Geophys Res Lett. https://doi.org/10.1029/2018gl079684

Sutton AJ, Wanninkhof R, Sabine CL et al (2017) Variability and trends in surface seawater pCO2 and CO2 flux in the Pacific Ocean. Geophys Res Lett 44:5627–5636. https://doi.org/10.1002/2017GL073814

Takahashi T, Olafsson J, Goddard JG et al (1993) Seasonal variation of CO 2 and nutrients in the high-latitude surface oceans: a comparative study. Global Biogeochem Cycles 7:843–878. https://doi.org/10.1029/93GB02263

Takahashi T, Sutherland SC, Wanninkhof R et al (2009) Climatological mean and decadal change in surface ocean pCO2, and net sea–air CO2 flux over the global oceans. Deep Res Part II Top Stud Oceanogr 56:554–577. https://doi.org/10.1016/j.dsr2.2008.12.009

Trenberth KE, Hurrell JW (1994) Decadal atmosphere-ocean variations in the Pacific. Clim Dyn 9:303–319. https://doi.org/10.1007/BF00204745

Tung K-K, Chen X, Zhou J, Li K-F (2019) Interdecadal variability in pan-Pacific and global SST, revisited. Clim Dyn 52:2145–2157. https://doi.org/10.1007/s00382-018-4240-1

Valsala V, Roxy M, Ashok K, Murtugudde R (2014) Spatiotemporal characteritics of seasonal to multidecadal variability of pCO2 and air–sea CO2 fluxes in the equatorial Pacific Ocean. J Geophys Res Ocean 119:8987–9012. https://doi.org/10.1002/2014JC010212.Received

Wang X, Christian JR, Murtugudde R, Busalacchi AJ (2006) Spatial and temporal variability of the surface water pCO2 and air–sea CO2 flux in the equatorial Pacific during 1980–2003: a basin-scale carbon cycle model. J Geophys Res Ocean 111:1–18. https://doi.org/10.1029/2005JC002972

Wang X, Le Borgne R, Murtugudde R et al (2008) Spatial and temporal variations in dissolved and particulate organic nitrogen in the equatorial Pacific: biological and physical influences. Biogeosciences 5:1705–1721. https://doi.org/10.5194/bg-5-1705-2008

Wang X, Murtugudde R, Hackert E et al (2015) Seasonal to decadal variations of sea surface pCO2 and sea-air CO2 flux in the equatorial oceans over 1984–2013: a basin-scale comparison of the Pacific and Atlantic Oceans. Global Biogeochem Cycles 29:597–609. https://doi.org/10.1002/2014GB005031

Wanninkhof R (1992) Relationship between wind speed and gas exchange. J Geophys Res 97:7373–7382. https://doi.org/10.1029/92JC00188

Wanninkhof R, Triñanes J (2017) The impact of changing wind speeds on gas transfer and its effect on global air–sea CO2 fluxes. Global Biogeochem Cycles 31:961–974. https://doi.org/10.1002/2016GB005592

Wanninkhof R, Asher WE, Ho DT et al (2009) Advances in quantifying air–sea gas exchange and environmental forcing. Ann Rev Mar Sci 1:213–244. https://doi.org/10.1146/annurev.marine.010908.163742

Wanninkhof R, Park GH, Takahashi T et al (2013) Global ocean carbon uptake: magnitude, variability and trends. Biogeosciences 10:1983–2000. https://doi.org/10.5194/bg-10-1983-2013

Wetzel P, Winguth A, Maier-Reimer E (2005) Sea-to-air CO2 flux from 1948 to 2003: a model study. Global Biogeochem Cycles 19:1–19. https://doi.org/10.1029/2004GB002339

Xiu P, Chai F (2014) Variability of oceanic carbon cycle in the North Pacific from seasonal to decadal scales. J Geophys Res Ocean 119:5270–5288. https://doi.org/10.1002/2013JC009505

Yu JY, Kim ST (2010) Identification of Central-Pacific and Eastern-Pacific types of ENSO in CMIP3 models. Geophys Res Lett 37:1–7. https://doi.org/10.1029/2010GL044082

Zhai P, Rodgers KB, Griffies SM et al (2017) Mechanistic drivers of reemergence of anthropogenic carbon in the equatorial pacific. Geophys Res Lett 44:9433–9439. https://doi.org/10.1002/2017GL073758

Zhang R-H (2015) An ocean-biology-induced negative feedback on ENSO as derived from a hybrid coupled model of the tropical Pacific. J Geophys Res Ocean 120:8052–8076. https://doi.org/10.1002/2015JC011305

Zhang R-H, Gao C (2016) The IOCAS intermediate coupled model (IOCAS ICM) and its real-time predictions of the 2015–2016 El Niño event. Sci Bull 61:1–10. https://doi.org/10.1007/s11434-016-1064-4

Zhang R-H, Levitus S (1997) Structure and cycle of decadal variability of upper-ocean temperature in the North Pacific. J Clim 10:710–727. https://doi.org/10.1175/1520-0442(1997)010%3c0710:SACODV%3e2.0.CO;2

Zhang R-H, Rothstein LM, Busalacchi AJ (1998) Origin of upper-ocean warming and El Niño change on decadal scales in the tropical Pacific Ocean. Nature 391:879–883. https://doi.org/10.1038/36081

Zhang R-H, Rothstein LM, Busalacchi AJ (1999) Interannual and decadal variability of the subsurface thermal structure in the Pacific Ocean: 1961–90. Clim Dyn 15:703–717. https://doi.org/10.1007/s003820050311

Zhang R-H, Tian F, Wang X (2018a) Ocean chlorophyll-induced heating feedbacks on ENSO in a coupled ocean physics-biology model forced by prescribed wind anomalies. J Clim 31:1811–1832. https://doi.org/10.1175/JCLI-D-17-0505.1

Zhang R-H, Tian F, Wang X (2018b) A new hybrid coupled model of atmosphere, ocean physics, and ocean biogeochemistry to represent biogeophysical feedback effects in the tropical Pacific. J Adv Model Earth Syst 10:1901–1923. https://doi.org/10.1029/2017MS001250